36403

National Library of Canada / Bibliothèque nationale du Canada

CANADIAN THESES ON MICROFICHE / THÈSES CANADIENNES SUR MICROFICHE

NAME OF AUTHOR/*NOM DE L'AUTEUR* YEHKAI HSIEH

TITLE OF THESIS/*TITRE DE LA THÈSE* TEMPERATURE MEASUREMENTS IN A TEA CO_2 AMPLIFIER

UNIVERSITY/*UNIVERSITÉ* UNIVERSITY OF ALBERTA

DEGREE FOR WHICH THESIS WAS PRESENTED/ *GRADE POUR LEQUEL CETTE THÈSE FUT PRÉSENTÉE* M. Sci.

YEAR THIS DEGREE CONFERRED/*ANNÉE D'OBTENTION DE CE GRADE* FALL, 1978

NAME OF SUPERVISOR/*NOM DU DIRECTEUR DE THÈSE* DR. A. M. ROBINSON

Permission is hereby granted to the NATIONAL LIBRARY OF CANADA to microfilm this thesis and to lend or sell copies of the film.

The author reserves other publication rights, and neither the thesis nor extensive extracts from it may be printed or otherwise reproduced without the author's written permission.

L'autorisation est, par la présente, accordée à la BIBLIOTHÈQUE NATIONALE DU CANADA de microfilmer cette thèse et de prêter ou de vendre des exemplaires du film.

L'auteur se réserve les autres droits de publication; ni la thèse ni de longs extraits de celle-ci ne doivent être imprimés ou autrement reproduits sans l'autorisation écrite de l'auteur.

DATED/*DATÉ* March 21, 1978 SIGNED/*SIGNÉ* Yehkai Hsieh

PERMANENT ADDRESS/*RÉSIDENCE FIXÉ* #6, 8550-82 AVE
EDMONTON, ALTA.
T6C 0Y8

NL-91 (3-74)

National Library of Canada

Cataloguing Branch
Canadian Theses Division

Ottawa, Canada
K1A 0N4

Bibliothèque nationale du Canada

Direction du catalogage
Division des thèses canadiennes

NOTICE

The quality of this microfiche is heavily dependent upon the quality of the original thesis submitted for microfilming. Every effort has been made to ensure the highest quality of reproduction possible.

If pages are missing, contact the university which granted the degree.

Some pages may have indistinct print especially if the original pages were typed with a poor typewriter ribbon or if the university sent us a poor photocopy.

Previously copyrighted materials (journal articles, published tests, etc.) are not filmed.

Reproduction in full or in part of this film is governed by the Canadian Copyright Act, R.S.C. 1970, c. C-30. Please read the authorization forms which accompany this thesis.

THIS DISSERTATION
HAS BEEN MICROFILMED
EXACTLY AS RECEIVED

AVIS

La qualité de cette microfiche dépend grandement de la qualité de la thèse soumise au microfilmage. Nous avons tout fait pour assurer une qualité supérieure de reproduction.

S'il manque des pages, veuillez communiquer avec l'université qui a conféré le grade.

La qualité d'impression de certaines pages peut laisser à désirer, surtout si les pages originales ont été dactylographiées à l'aide d'un ruban usé ou si l'université nous a fait parvenir une photocopie de mauvaise qualité.

Les documents qui font déjà l'objet d'un droit d'auteur (articles de revue, examens publiés, etc.) ne sont pas microfilmés.

La reproduction, même partielle, de ce microfilm est soumise à la Loi canadienne sur le droit d'auteur, SRC 1970, c. C-30. Veuillez prendre connaissance des formules d'autorisation qui accompagnent cette thèse.

LA THÈSE A ÉTÉ
MICROFILMÉE TELLE QUE
NOUS L'AVONS REÇUE

NL-339 (3/77)

THE UNIVERSITY OF ALBERTA

TEMPERATURE MEASUREMENTS IN A TEA CO_2 AMPLIFIER

by

YEH KAI HSIEH

©

A THESIS

SUBMITTED TO THE FACULTY OF GRADUATE STUDIES AND RESEARCH

IN PARTIAL FULFILMENT OF THE REQUIREMENTS FOR THE DEGREE

OF MASTER OF SCIENCE

DEPARTMENT OF ELECTRICAL ENGINEERING

EDMONTON, ALBERTA

SPRING, 1978

THE UNIVERSITY OF ALBERTA

FACULTY OF GRADUATE STUDIES AND RESEARCH

The undersigned certify that they have read, and recommend to the Faculty of Graduate Studies and Research, TEMPERATURE MEASUREMENTS IN A TEA CO_2 AMPLIFIER

submitted by YEH KAI HSIEH

in partial fulfilment of the requirements for the degree of Master of Science.

A. W. Robinson
Supervisor

Date March 14, 1978

ABSTRACT

An accurate measurement of gas temperature in a CO_2-He-N_2 amplifier at 1 atmosphere which employs volumetric photoionization of the gas by ultraviolet radiation has been performed by measuring the absorption of a CO_2 laser beam. The temperature was determined not from a computed absorption coefficient but from the experimentally known data relating the absorption coefficient and temperature, for the specific gas mixes which are CO_2:He:N_2= 30:55:15 and 13:77:10. This auxiliary experiment has been performed to avoid the problem of uncertainties in lineshapes, wavelengths and transition probabilities inherent in a computed value of the absorption coefficient. Comparisons are also made between the calculated absorption coefficient and experimental measurements.

Temperatures in the range 400 - 600 K have been observed at the center between the uniform field electrodes using applied voltages from 35 to 60 kV. The temperature decreased from the center of the discharge towards the sides, and was initially constant along the direction of the transverse current. A temperature increase was observed with input energy, while a decrease was found with pressure, decay time, distance between electrodes, and flatness of the electrode profile. Estimation of energy deposition into the discharge showed that 75% of the total input energy heats the gas. A temperature of approximately 450 K was optimum for maximizing the small-signal gain in this system.

ACKNOWLEDGMENT

The author wishes to acknowledge the assistance provided by Dr. A.M. Robinson during the course of this thesis. Assistance from Mr. B. Haverstock, Mr. K. Doerrbecker, and Mr. H. Ganns is also gratefully acknowledged.

The work described in this thesis was performed under support from the Deference Research Board of Canada whose assistance is gratefully acknowledged.

The author also extends a special acknowledgment to his wife, Gloria Hsieh, whose diligence and patience during the course of this thesis and the typing of the manuscript are greatly appreciated.

TABLE OF CONTENTS

		Page
CHAPTER 1	INTRODUCTION	1
CHAPTER 2	ABSORPTION COEFFICIENT MEASUREMENTS	5
	2.1 Theory and Computation	5
	2.1.1 Theory	5
	2.1.2 Computation	7
	2.2 Experimental Method	11
	2.2.1 Experimental Set-up	11
	2.2.2 Experimental Method	12
	2.3 Results of Absorption Experiment	14
	2.4 Discussion of Results	15
CHAPTER 3	TEMPERATURE MEASUREMENTS IN A TEA CO_2 AMPLIFIER	18
	3.1 Experimental Set-up and Experimental Procedure	18
	3.1.1 Experimental Set-up	18
	3.1.2 Experimental Procedure	21
	3.2 Results and Discussion	22
	3.3 Energy Estimation	27
	3.4 Errors	30
	3.5 Correction of Temperature Measurements	32

		Page
CHAPTER 4	CONCLUSIONS AND SUGGESTIONS FOR FURTHER RESEARCH	34
	4.1 Summary of Results and Conclusions	34
	4.2 Suggestions for Further Research	35

LIST OF TABLES

		Page
Table 1	The Coefficients of the Cubic Polynomial of k as a Function of T for Three Wavelengths and Two Different Mixtures.	15
Table 2	Details of Energy Estimation for Input Voltage= 50 kV.	29
Table 3	Summary of the Percentage of the Deposited Energy for the Input Voltage from 35 to 60 kV.	30

LIST OF FIGURES

		Page
Figure 1	Schematic Diagram of Absorption Measurement Configuration.	38
Figure 2	Small Signal Absorption Coefficient of Various R and P Branch CO_2 Laser Transitions in The 10.6 μm Band at 310 K in 100:0:0 Mix.	39
Figure 3	Small Signal Absorption Coefficient at Various Pressures for P(20) at 310 K and M= 100:0:0.	40
Figure 4	Absorption Coefficient as A Function of Temperature for P(20) in Pure CO_2(M= 100:0:0).	41
Figure 5	Absorption Coefficient as A Function of Temperature for P(20) in Gas Mix(M= 30:55:15).	42
Figure 6	Absorption Coefficient as A Function of Temperature for P(20) in Gas Mix(M= 13:77:10).	43

		Page
Figure 7	Standard Curve of Absorption Coefficient Against Temperature for P(20), P(22), P(18) at M= 30:55:15.	44
Figure 8	Standard Curve of Absorption Coefficient Against Temperature for P(20), P(22), P(18) at M= 10:77:13.	45
Figure 9	Schematic Diagram of Temperature Measurement Configuration.	46
Figure 10	a. Amplifier and Discharge Circuit Diagram. b. Cross Section of Four Electrode Shapes.	47
Figure 11	Oscilloscope Traces of Temperature Measurement.	48
Figure 12	Temperature Profile with x Position.	49
Figure 13	Temperature Profile with y Position.	50
Figure 14	Temperature Profile with Pressure.	51
Figure 15	Temperature Decay with Time.	52

Page

Figure 16 Temperature Decay with Time. 53

Figure 17 Temperature Profile with x Position. 54

Figure 18 Temperature Profile with x Position. 55

Figure 19 Temperature Profile with x and y Position. 56

Figure 20 Temperature Profile with x and y Position. 57

LIST OF SYMBOLS

A_{21} - Einstein's spontaneous transition probability

B_i - rotational constant of the mode i

C - main discharging capacitor

c - pin discharging capacitor

C_p - specific heat at constant pressure

d - distance between two electrodes

E - total heat energy

F_J - interation factor between vibration and rotation

$G(\nu)$ - normalized lineshape function

g_2 - statistical weight in upper level

g_1 - statistical weight in lower level

g - distance between two pin capactitors

h - Planck's constant = 6.6356×10^{-27} erg sec

I_ν - intensity of a monochromatic plane wave

I_m - main current through the electrode-gap

I_t - total current through the discharge-system

I_p - pin current through the capacitor c

I_s - saturation intensity

i - 3 fundamental vibrational modes of CO_2

J - rotational quantum number

K - Boltzmann's constant = 1.3805×10^{-16} erg$(K)^{-1}$

k - small signal absorption coefficient

kV - unit of applied voltage = 1000 volts

L - length of the absorption cell

l - orbital angular-momenta quantum number

m - rotational quantum number = $-J$

N - total number density of CO_2 molecules

N_o - Avogadro's number = 6.602252×10^{23} $mole^{-1}$

N_1 - number density in lower level

N_2 - number density in upper level

N_{iJ} - number density in level J for the mode i

N_{iV} - number density in level V for the mode i

p - pressure

Q_V - vibrational partition function

Q_{iR} - rotational partition function for the mode i

R_{12} - transition moment between two levels

S_J - rotational factor

T_i - gas temperature following the discharge

T_o - room temperature

t - thickness of the electrode

V - vibrational quantum number

W_{12} - induced transition rates per atom between two levels

W - width of the electrode

w - total width of the electrode with pin capacitors

w_i - vibrational frequencies of the mode i

α_o - small-signal gain coefficient

β - transmission of the laser beam

β' - apparent transmission of the laser beam

γ_k - relative error of the absorption coefficient k

γ_β - relative error of the transmission of the laser beam β

γ_L - relative error of the absorption length L

$\Delta \nu_L$ - FWHM due to Lorentz broadening

$\Delta \nu_D$ - FWHM due to Doppler broadening

ϵ - energy density in the discharge volume

θ_j - fractional contents of component j in the gas mixture

λ - wavelength

μm - micrometer = 10^{-4} cm

ν - frequency

ρ - gas density

CHAPTER 1

INTRODUCTION

Gas temperature has been recognized as one of the important properties determining laser output. A high temperature results in an increase in the population density of the lower laser level with subsequent reduction in gain. Gordietz et al. [1] pointed out that in order to sustain a population inversion in the low pressure CW CO_2 laser, the gas temperature was limited typically to 600 K. For the pulsed TEA CO_2 laser [2], if the laser pulse cannot be emitted rapidly enough before equilibrium is completely established between electronic, vibrational, rotational and kinetic energies, then limitiation on the gas temperature would be similiar to the CW-laser case.

More specifically, the performance of a CO_2 laser is characterized by the values of the small-signal gain α_o and the saturation intensity I_s [3]. The former is the fractional increase of the intensity of an infinitesimal 10.6 μm radiation flux per centimeter of the plasma traversed by the radiation, and the latter is the value of the radiation intensity for which the gain is reduced to one-half of α_o. The product of α_o and I_s is the maximum available output power density.

The variation of α_o and I_s with gas temperature and electron density has been calculated in the paper of Fowler[4]

by using the kinetic models proposed by Gordietz et al. [1] and by Moore et al. [5]. The results show that the optical power density increases with increasing electron density as long as the gas temperature remains low. However, the strong deleterious effect of rising gas temperature on α_o causes the output power density to decrease with increasing temperature in spite of the increase in electron density. Some numerical values show the optical power density approaches zero even for values of electron density in excess of $10^{10} cm^{-3}$ if the gas temperature is greater than approximately 700 K.

Hence, knowledge of the kinetic temperature of the gas in a TEA CO_2 laser is important for two principal reasons. First, in a single pulse TEA CO_2 laser, the duration and amplitude of the gain pulse can decrease if the gas temperature increases excessively by pumping greater amounts of energy into the gas [6],[7]. Secondly, in regard to high repetition rate CO_2 TEA lasers, the repetitive glow discharge becomes unstable when undesired gas discharge products, due to gas heating, remain in the interelectrode region throughout the time interval between current pulses [8]. For this reason, ample time between pulses must occur in order to avoid any cumulative rise in gas temperature. Therefore, a prerequisite of the design of a high repetition rate CO_2 TEA laser would be a gas flow system to sustain a constant low gas temperature.

Measurement of the gas temperature in a sealed CO_2 discharge system has been reported using interferometric

methods [9],[10], but having little time and space resolution. Measuring the small-signal gain during the gain pulse will allow a determination of the rotational temperature in the low-pressure [11] and high-pressure regimes [12]-[17]. Due to the fast relaxation between rotation and translation, the kinetic and rotational temperatures are assumed equal, and a mathematical expression for the gain coefficient is derived from which the temperature may be extracted along with the upper and lower level population densities. This method depends on accurate values of spectroscopic and collision constants.

Another method for measuring the equilibrium kinetic temperature following the gain has been to observe the absorption of 10.6 μm radiation by the hot CO_2 [14]. The absorption coefficient is calculated as a function of temperature, from which the latter quantity can be obtained. This method, too, relies on accurate spectroscopic and collisional data for CO_2. However, recent experimental results [18] have shown that a simple two-level model of the absorption process is not accurate at elevated temperatures and overlap of several transitions must be considered.

Laser devices must be designed to operate at an optimum temperature in order to produce maximum laser output power. Therefore, the purpose of this experiment is to measure the amount of heating that occurs in a TEA CO_2 laser amplifier after the discharge, and especially the temperature rise and decay as a function of time and position. Once the

temporally and spatially resolved temperature has been measured, we can determine the optimum condition for high gain performance.

The method of temperature determination described in this thesis involved the absorption of 10.6 μm radiation following the discharge and gain in the amplifier. The temperature, however, was determined not from a computed absorption coefficient but from the experimentally measured variation of the absorption coefficient with temperature, for the specific gas under consideration. The variation of the absorption coefficient k with temperature T was measured in an auxiliary experiment, and avoids the problem of uncertainties in linewidths, wavelengths, and transition probabilities inherent in a computed value of the absorption coefficient. This auxiliary experiment is described in Chapter 2.

In Chapter 3, equilibrium temperature measurements carried out in a UV-sustained TEA CO_2 amplifier using the experimental data from Chapter 2 is presented. Details of the experimental set-up and variations of temperature with spatial position in both the x and y directons, electrode shape and distance, pressure, discharge voltage and time will be described. Discussions of these results will also be made.

A summary of results and conclusions as well as suggestions for further research will be outlined in Chapter 4.

CHAPTER 2

ABSORPTION COEFFICIENT MEASUREMENTS

2.1 Theory and Computation

2.1.1 Theory

Consider the case of a monochromatic plane wave of frequency ν and intensity I_ν propagating through an atomic medium with N_2 atoms per unit volume in level 2 (upper level) and N_1 in level 1 (lower level). There will occur N_2W_{21} induced transitions per unit time per unit volume from level 2 to level 1 and N_1W_{12} transitions from 1 to 2. Therefore, the intensity grows when the population is inverted ($N_2 > N_1$) or attenuates when the population is not inverted ($N_2 < N_1$). The former case corresponds to laser amplification, the latter case absorption. The net power generated within a unit volume is [19]

$$\frac{P}{\text{volume}} = \left(N_2 - \frac{g_2}{g_1} N_1\right) W_{21} h\nu$$

Where g_2, g_1 are the statistical weights in the upper and lower levels, W_{21} and W_{12} are transition rates per atom between the upper and lower levels, equal to $\frac{\lambda^2 I_\nu}{8\pi h\nu} A_{21} G(\nu)$ [20], A_{21} is Einstein's spontaneous transition probability, $G(\nu)$ is the normalized lineshape function and λ is the wavelength corresponding to frequency ν. In the absence of

any power dissipation, this radiation will be added coherently (that is, with a definite phase relationship) to that of the traveling plane wave so that it is equal to the increase in the intensity per unit length, or:

$$\frac{dI_\nu}{dz} = \left(N_2 - \frac{g_2}{g_1} N_1\right) \frac{\lambda^2 I_\nu}{8\pi} A_{21} G(\nu)$$

If we let

$$k(\nu) = -\frac{\lambda^2}{8\pi} A_{21} \left(N_2 - \frac{g_2}{g_1} N_1\right) G(\nu) \qquad (1)$$

then $$\frac{dI_\nu}{dz} = -k(\nu)\, I_\nu$$

and assuming a small signal so that N_1 and N_2 remain constant, the solution is

$$I_\nu (z) = I_\nu (0) \exp (-k(\nu)z)$$

$I_\nu (z)$ and $I_\nu (0)$ can be measured experimently with detectors in the laboratory and hence the measurement of $k(\nu)$ can be made:

$$k (\nu) = \frac{-\ln \beta}{L} \qquad (2)$$

where $\beta = \frac{I_\nu(z)}{I_\nu(0)}$ = transmission of the laser beam and L = length of the absorption cell

2.1.2 Computation

The theoretical calculation of absorption coefficient as a function of temperature can be made for comparsion with the experimental measurement. Each factor in eq. (1) will be considered in what follows, using recent experimental data.

2.1.2.1 Wavelenth λ

The most accurate values of the wavelength in the P and R branches of both the 00°1 - 10°0 and 00°1 - 02°0 bands of CO_2 are reported by Petersen et al. [21] and Chang [22]. Here we are using the P(20) line (λ= 10.591 μm) in the computation.

2.1.2.2 Spontaneous Transition Probability A_{21}

The spontaneous transition probability is given by [23]

$$A_{21} = \frac{64\,\pi^4}{3h\lambda^3} \quad \frac{|R_{12}|^2 S_J F_J}{g_2}$$

Where $|R_{12}|^2$ is the vibrational contribution to the transition moment, S_J is the rotational contribution, and F_J is the interaction factor between vibration and rotation.

The most recent determination of $|R_{12}|$ [24] gives the value $(4.01 \pm 0.01) \times 10^{-20}$ statcoul-cm for the 00°1 - 10°0 transition. Values for the other factors are:

$F_J = 1 - 0.0022\ m$

$S_J = |m|$

$m = -J$ for a P branch transition

$J = 20$, referring to the lower laser level

$J' = 19$, referring to the upper laser level

$g_2 = 2\,J' + 1 = 39$

$g_1 = 2\,J + 1 = 41$

2.1.2.3 Population Densities N_1, N_2

The population densities are calculated under the assumption that Fermi resonance is negligible, the harmonic oscillator approximation is valid, vibrational-rotational interaction is negligible, and l-doubling in also negligible. According to Gray and Selvidge [25], these simplifications result in errors of less than 2% in computation of the partition function for temperatures up to 1200 K.

The vibrational level population density of vibrational mode i of CO_2 having vibrational quantum V is given by [26]

$$N_{iV} = \frac{N}{Q_V} \exp\left(-\frac{Vw_i hc}{KT}\right) \quad \begin{pmatrix} V = 0,1,2, \ldots \\ i = 1,3 \end{pmatrix}$$

Where N= total number density of CO_2 molecules, and variation with temperature, T and pressure, p is given by

$$N = \left(\frac{N_o}{22413.6\ \text{cm}^3\ \text{mole}^{-1}}\right)\left(\frac{p}{760\ \text{torr}}\right)\left(\frac{T}{273.16\ \text{K}}\right)^{-1}$$

N_o = Avogadro's number, 6.02252×10^{23} mole^{-1}, w_i are the

vibrational frequencies of the 3 fundamental vibrational modes of CO_2, namely

$w_1 = 1388.2\ cm^{-1}$

$w_2 = 667.4\ cm^{-1}$

$w_3 = 2349.2\ cm^{-1}$

Q_V is the vibrational partition function [27], given in the harmonic oscillator approximation, as

$$Q_V = \left[\left(1-e^{-\frac{w_1 hc}{KT}}\right)\left(1-e^{-\frac{w_2 hc}{KT}}\right)^2 \left(1-e^{-\frac{w_3 hc}{KT}}\right)\right]^{-1}$$

For the rotational levels superimposed on each vibrational level, the population density in level J is given by

$$N_{iJ} = \frac{N_{iV}}{Q_{iR}} \left(2J + 1 \right) e^{-\left[B_i J(J+1) \right] \frac{hc}{KT}}$$

here, Q_{iR} is the rotational partition function, given approximately by [28]

$$Q_{iR} \approx \frac{KT}{2hcB_i}$$

The most accurate values of B can be found in Refs. [21], [22].

$B_1 = 0.38988\ cm^{-1}$

$B_3 = 0.38684\ cm^{-1}$

2.1.2.4 Normalized Lineshape Function G(ν)

The normalized lineshape function for combined Doppler and Lorentz broadening is given by [29]

$$G(\nu) = \frac{2}{\pi^{3/2}\,\Delta\nu_L}\int_{-\infty}^{\infty} \frac{a^2 e^{-t^2}\,dt}{a^2 + (b-t)^2}$$

Where

$$a = \frac{\Delta\nu_L}{\Delta\nu_D}(\ln 2)^{\frac{1}{2}}$$

$$b = 2\left(\frac{\nu - \nu_o}{\Delta\nu_L}\right) a$$

$\Delta\nu_D$ is the full-width at half maximum (FWHM) of the spectral line due to Doppler broadening, written as $\frac{2\nu_o}{c}(2\frac{KT}{m}\ln 2)^{\frac{1}{2}}$ and $\Delta\nu_L$ is the width of the spectral line (FWHM) due to Lorentz broadening, given by [30]:

$$\Delta\nu_L = 7.58(\theta_{CO_2} + 0.73\,\theta_{N_2} + 0.64\,\theta_{He})\,p\left(\frac{300}{T}\right)^{\frac{1}{2}} \text{ in MHZ}$$

here, θ_j is the fractional content of component j in the gas mixture, p is the total pressure in torr, and T is the absolute temperature. At the line center (i.e. $\nu = \nu_o$), $G(\nu)$ reduces to [31]

$$G(\nu_o) = \frac{2}{\pi^{\frac{1}{2}}\,\Delta\nu_L}\, a e^{a^2}(1 - \text{erf } a)$$

For the pressures involved in this experiment, the dominant processes is Lorentz broadening, (i.e. $a \rightarrow \infty$)

$$G(\nu_o) = \frac{2}{\pi\,\Delta\nu_L}$$

The variation of line width with temperature is expected to follow a simple $T^{-\frac{1}{2}}$ relationship from considering

an elementary model of collision processes in the pressure-broadened regime [32]. However, experimental results [33] show this expectation is not correct. At high temperature the absorption coefficients may have contributions due to the overlapping of other transitions with wavelengths near that of the P(20) line. Further details will be presented at the end of this Chapter. Therefore, the computed values of absorption coefficient should be less than the experimental data in the high temperature region.

2.2 Experimental Method

2.2.1 Experimental Set-up

A schematic diagram of the apparatus employed in measuring the absorption coefficient over the temperature range 300 - 600 K in a cell is shown in Figure 1. A low-pressure, single transverse mode (TEM_{oo}) CW CO_2 laser served as the source. Its wavelength was selected by an intracavity grating and output power was slightly below 1 W. The radiation passed through a mechanical chopper, an absorption cell enclosed by the ceramic oven, a spectrum analyzer and finally was focused by a lens on a Ge (Au) detector (#1). The spectrum analyzer was used to continuously monitor the wavelength of the laser beam. A beam-splitter placed in front of the absorption cell deflected approximately half the beam onto a second Ge (Au) detector (#2). The reason for this was to ensure that any variation of the laser output intensity during the measurement could be accounted for, provided the signal

from the two detectors varied in the same manner when the laser intensity varied. The square wave signals from both detectors were monitored on an oscilloscope and two digital AC voltmeters.

The absorption cell was constructed from 2.5 cm ID stainless steel tubing with commercial bakeable barium fluoride windows, each 1.27 cm in diameter made by Harshaw Chemical Co., and attached to flanges at each end. The distance between the windows was 92 cm. A stainless steel tube connected the absorption cell to manometers, a gas mixing tank, gas bottles, and a mechanical pump. Mixing of CO_2: He:N_2 was achieved in a tank stirred by a series of propellers, mounted on a central rod and rotated by a electric motor. Seven theromocouples, one attached every 15 cm along the outside of the absorption cell, were used for monitoring the temperature along the length of the cell. The oven consisted of four half-round ceramic electric heating units of total length 150 cm and inner diameter 10 cm. The ceramic heating units were completely encased in glass wool insulation and enclosed in an aluminum container. The temperature in the oven was varied using a Variac connected across the heating units, and monitored with a digital voltmeter, connected sequentially to the seven thermocouples.

2.2.2 Experimental Method

The procedure followed in measuring the transmission of the CO_2 gas mixes was to start with the oven at room

temperature, pump out the absorption cell with the mechanical pump, and record the two signals shown on the voltmeters. The gas was then let into the cell to a pressure of 100 torr, and the two detector readings were again noted. Following this, the pressure was increased up to 700 torr in steps of 100 torr with the voltmeter readings being recorded at each step. Next the gas pressure was reduced again to 100 torr in steps of 100 torr. This process was then repeated for a different laser wavelength, the region of interest being around the P(20) line. Simultaneously power was applied to the oven heating elements, and the temperature was monitored through observation of the thermocouple voltages. The above measurements were then repeated at each temperature increase of approximately 25 K with the power to the heater elements slightly increased from time to time. Thus, the temperature increased monotonically during the time of measurements; however the temperature increase was less than 5 K during each set of measurements from 100 to 700 torr and back to 100 torr. Each set of measurements took approximately 3.5 minutes, long enough to allow the gas to reach thermal equilibrium; no significant variation of absorption coefficient k was observed during the course of a single set of measurements to indicate that k was changing because of an increasing temperature; furthermore, rough computations of heat-transfer times and amount of heat required to raise the temperature of the gas confirmed this conclusion. The ratio of the signal from detector (#1) when there was gas in the

absorption cell to when there was no gas in the cell was used to calculate the absorption coefficient k from eq.(2) above.

2.3 Results of Absorption Experiment

A diagram of the small signal absorption coefficient of various R and P branch CO_2 laser transitions in the 10.6 μm band at 310 K and a 100:0:0 mixture can be seen in Figure 2. Similiar measurements taken by Arié *et al.*[24] are also shown on the diagram.

Figure 3 shows the absorption coefficient against pressure for P(20) at 310 K in pure CO_2. Data from Ref. [24] is also shown.

Figures 4 - 6 presents the absorption coefficient against temperature from the experimental measurements and the theoretical calculation at line center. These results are summarized in Figures 7 and 8, which are least-squares fits of a cubic polynomial of the data of Figures 5 and 6. The coefficients of the polynomial for three wavelengths and two different mixtures is given in Table 1. These curves were subsequently used in measuring the gas temperature in the TEA CO_2 laser amplifier. The horizontal error bars, shown in Figures 4 - 6, representing the uncertainty in T indicate the standard deviation of the seven thermocouple readings. At 580 - 600 K, the deviation in the seven temperatures was approximately 10 K. The vertical bars represent upper bounds on the expected error in k, which will be discussed in Section 3.4.

Table 1 The Coefficients of the Cubic Polynomial of k as a Function of T for Three Wavelengths and Two Different Mixtures.

$$k = AT^3 + BT^2 + CT + D$$

CO_2:He:N_2	λ	A($\times 10^{-10}$)	B($\times 10^{-7}$)	C($\times 10^{-4}$)	D($\times 10^{-1}$)
30:55:15	P(20)	-2.085	2.937	-1.074	0.123
	P(22)	-2.174	2.996	-1.108	0.129
	P(18)	-1.571	2.105	-0.698	0.070
13:77:10	P(20)	-0.612	0.859	-0.293	0.030
	P(22)	-0.363	0.558	-1.823	0.016
	P(18)	-0.134	0.211	-0.231	0.007

2.4 Discussion of Results

As the vibrational-rotational transition was changed in the probe laser, the peak values of k shown in Figure 2 were recorded for the pure CO_2 at 310 K. Both the P and R branch absorption coefficient attained their maximum values for lower level values of $J \approx 16$. From the Boltzmann distribution of the population density N_J of the various rotational levels, the level at which N_J is a maximum is given by [34]

$$J_{max} = \left(\frac{KT}{2hcB} \right)^{\frac{1}{2}} - \frac{1}{2}$$

here, if we put $J_{max} = 16$ we obtain a temperature T= 306 K and $J_{max} = 18$, T= 381 K, The temperature is only accurate to within 22% and this relation assumes that a simple 2-level model of absorption is valid.

In Figure 3, it can be seen that the measured absorption coefficient was independent of the gas pressure for P(20) except in the lower pressure region ($p \leq 20$ torr).

In the Doppler broadened region the absorption coefficient is proportional to the gas pressure because both N_2 and N_1 are directly proportional to pressure and in the case of collision broadening, the absorption coefficient should be independent of pressure due to the normalized line shape $G(\nu)$ being inversely proportional to the pressure. From eq. (1), we can see both presure-dependent factors will cancel each other. Similiar results are presented in the paper by Arié et al. [24].

It was first noticed by Ely and McCubben [33] that the temperature variation of linewidth in pure CO_2 did not follow a simple $T^{-\frac{1}{2}}$ relationship as might be expected from an elementary model of collision processes in the pressure broadened regime. Recent experimental data by Leonard [18] for temperatures up to 600 K, and in a higher temperature range by Strilchuk and Offenberger [35] have confirmed the discrepancy. Figures 4 - 6 show the measured absorption coefficient against temperature for pure CO_2 and the gas mix used in the succeeding experiment. The theoretical computations of the 2-level absorption model discussed in section 2.1.2 were also included for comparison. In the pure CO_2 case some of Leonard's results [18] have also been plotted at two different pressures. The agreement between our results and those of Leonard are satisfactory considering the spread in his values.

It has been suggested by Munjee and Christensen [36] that the transistions between the $01^11 - 11^10$ levels and the $02^01 - 12^00$ levels also contribute to the absorption.

Their calculations give satisfactory agreement with Leonard's measured data. Unfortunately, the absolute magnitude of the mixed mode contributions are questionable primarily because the rotational-vibrational constants of the molecule are not known with adequate precision. Despite this, the measurements show that in pure CO_2 the P(20) absorption coefficient did not vary with pressure over a range from 100 to 700 torrs, within the experimental errors. This is contrary to the calculations of mixed mode absorption considered in Ref. [36]. This suggests that the linewidths, wavelengths or the pressure broadening coefficients of the overlapping absorption lines are not known accurately enough. More precise measurement are currently being under taken to further clarify this discrepancy [37].

CHAPTER 3

TEMPERATURE MEASUREMENTS IN A TEA CO_2 AMPLIFIER

3.1 Experimental Set-up and Experimental Procedure

3.1.1 Experimental Set-up

Figure 9 is a schematic diagram of the apparatus used for this experiment. A low-pressure CW CO_2 laser was operated in the fundamental mode. (TEM_{oo}) An internal grating allowed the output to be tuned over several lines in the P branch of the 10.6 μm band. The output beam had a power of approximately 1 W. This probe beam was chopped by a mechanical chopper and reflected from adjustable mirrors, passed through the amplifier and then focused onto a Ge(Au) detector. A beamsplitter located between two mirrors was used to deflect the beam into a CO_2 spectrum analyzer to monitor the wavelength. The diameter of the laser beam was limited in front of the amplifier by a 5 mm iris to obtain better spatial resolution. A 10 cm focal length lens was used in front of the detector to focus the beam onto the detecting element. The reason for the lens was to minimize the effects of deflection of the laser beam due to nonuniform heating of the gas in the amplifier. Without the lens, large distortions were evident for 10 milliseconds or more after the discharge; with the detector at the focus of the lens, a minimum amount of distortion occurred and only for the first few milliseconds.

The exact geometrical structure of the amplifier has been described by Robinson [6] in his laser gain measurements. Briefly, the amplifier consisted of a two stage Marx bank circuit connected to the Chang profile electrodes [38]. The gap between the electrodes was preionized by UV radiation which in turn was produced by intense arcs conducted through capacitors and pin electrodes connected in parallel with the main electrodes and situated every 10 cm along their length. The system was similiar to that described by Burnett and Offenberger [39] but with the capability of wider electrodes (up to 18 cm), adjustable arc lengths and distance from the main electrodes, and variable pressure, although most measurements were performed at 1 atmosphere. Figure 10 is a schematic diagram of the electrodes and discharge circuit. The important parameters of the amplifier are: electrode length L= 58 cm, d= 5.1cm, W= 13 cm, w= 18 cm, g= 1.8 cm, t= 2.5 cm, C= 0.1 μF and c= 570 pF. The pertinent discharge currents are labelled. The applied voltage was varied from 35 to 60 kV, the lower limit governed by the onset of arcs in the discharge and the upper by the power supply. A mechnical fan mounted in PVC pipe on top of the amplifier circulated the gas along the axis of the amplifier to ensure good mixing of the three gases. Helium, Carbon Dioxide and Nitrogen passed through separate flow meters, were mixed, and then flowed into the amplifier in the negative x-direction and finally out into the laboratory. The average velocity of the gas was 2.15 cm/min for 30:55:15 and 3.22 cm/min for

13:77:10 through the discharge volume. Two NaCl windows, tilted at a small angle to avoid reflections back into the laser, were mounted on both ends of the amplifier.

The electrode material was Union Carbide AGOT grade graphite stock with a resistivity of 6.5×10^{-4} ohm-cm. The ends of the electrode were semi-circular and the technique of shaping and cutting the electrode has been described by Seguin et al. [40]. The uniform field profiles described by Chang [38] and used in these measurements depend on a parameter k (not to be confused with the absorption coefficient k) which can be related directly to the curvature of the profile only under special conditions. In general terms, however, the lower the value of k the flatter is the electrode and the more uniform is the electric field between the electrodes. From the point of view of the glow-to-arc transitions, the discharge performance was best for a separation of 5.1 cm for the particular operating conditions used in this experiment, although measurements were also performed for d= 4.3 cm and 5.8 cm. Four electrode profiles were studied in this investigation, having a value of k= 0.07, 0.05, 0.03 and 0.00. The electrodes will henceforth be referred to as electrodes 7, 5, 3 and 0 respectively.

The predicted electrode profile extends beyond the width W of the electrode. Rather than ending the profile abruptly at the junction of the vertical side and the profile surface, a smooth but somewhat arbitrary round-off of the edge was performed. Without rounding, the electrodes with low k

values tended to arc at this edge. The radii of curvature of the rounding was approximately 0, 0.9, 0.9 and 1.9 cm for electrodes 7, 3, 5 and 0 respectively. The cross sections of the four electrodes are shown in Figure 10b. The profiles are symmetric about the center line. The region of round-off is indicated with the exact shape extending to the edge of the electrode marked by a dashed line. More details about the calculation and configuration of the profiles are given by Chang [38]. The whole discharge sequence in the amplifier has also been described in the paper by Robinson [6].

3.1.2 Experimental Procedure

The procedure followed in making these measurements was to record two successive traces of the oscilloscope. The first trace of the chopped laser beam occured without a discharge in the amplifier and immediately after this, a second trace with a discharge in the amplifier. The measurement made with a discharge would show initially the large increase in laser signal due to amplification for a few microseconds after the discharge, and was then followed by a substantial decrease in signal due to absorption. The time evolution of the absorption signal could then be monitored on a time scale set according to the sweep speed of the oscilloscope. Figure 11 shows four such measurements at different sweep speeds. The initial transmission after the gain pulse, as indicated by the traces in Figure 11a, 11b and 11c is approximately 83%, while 11d indicates a return to normal temperatures in

approximately 50 ms. A correction to the absorption coefficient computed from the ratio of the two signals must be applied because the "non-absorbed" trace in fact represents the transmission through the gas mix at room temperature (see section 3.5). The correction amounts to adding the value of the absorption coefficient at room temperature for the particular gas mix, as measured in the previous experiment, to the apparent absorption coefficient calculated from the data of Figure 11.

Following the above procedure, measurements of absorption and hence temperature in the TEA CO_2 amplifier were made as a function of position in the horizontal (x) and vertical (y) directions, pressures, electrode shapes, discharge voltages and electrode separations. Simultaneous voltage and current measurements were also attempted in order to compute energy deposited into the gas during the discharge. Unfortunately, the voltage measurements were not successful. Because of the high voltage involved, special voltage dividers were constructed which did not remain linear under high voltage operation and the amount of nonlinearity could not be accurately determined. An indirect method of calculating this energy will be presented in section 3.3.

3.2 Results and Discussion

The variation of temperature with position in the horizontal (x) direction midway between the two electrodes in the amplifier is shown in Figure 12. The experimental

conditions are indicated in the diagram. The time at which the temperature was measured was 3.6 ms after the discharge. The temperature profiles shown in Figure 12 are labelled according to the charging voltage placed on the capacitors in the amplifier, which are connected in a voltage doubling circuit. It can be seen that as the charging voltage increases, and hence the input energy into the gas increases, the temperature at any position increases, as one would expect. As was observed for the small-signal gain [6] a slight asymmetry of the temperature profiles can be seen. The reason for this phenomenon is not known. Typical error bars are also shown representing the expected error in T.

A similiar set of temperature profiles is shown in Figure 13, taken under the same conditions as the previous figure, but now the measurements were made in the vertical (y) direction in a plane midway between the sides of the electrodes. It can be seen that the temperature is constant in the y-direction except in the regions close to the electrodes. This general behavior was also observed with the small-signal gain [6]; the variation of temperature near the electrodes can probably be accounted for by rapid electric field and electron density variations in the electrode sheath regions as well as the proximity of the cold electrode. The 5-mm-diameter laser beam could not provide good spatial resolution in these regions for detailed measurements.

Figure 14 indicates the variations of temperature at the center of the discharge with gas pressure, for the 30:55:15 gas mix, at various applied voltages as indicated, for the

P(20) line. The measurement was made 5 ms after the discharge in the amplifier. As anticipated, the temperature rise was greater the higher the charging voltage, and the lower the pressure. Temperatures above 600 K were estimated by extrapolating the cubic curves of temperature of Figure 7. If the discharge volume and input energy to the gas are independent of the pressure, then the temperature increase would vary inversely with gas density and hence vary inversely with the pressure (also assuming the specific heat is not a function of temperature, which is approximately true). The dotted curve in Figure 14 varies in this manner, passing through the 35 kV curve at 100 torr. In fact, the measurements show that less energy is being deposited into the gas at low pressures than at high pressures. Indeed it has been observed in a resistive-pin CO_2 TEA laser that the energy input does decrease with decreasing pressure [7], and this appears to be the case here. However, it is also possible that the discharge is more spread out at lower pressures, which would also contribute to the divergence from a p^{-1} relation.

The variation of temperature for the six charging voltages as a function of time following the discharge is shown in Figure 15. The temperatures shown are those measured at the center of the discharge, starting approximately 1.5 ms after the discharge and extending up to 48 ms. The temperature drops off monotonically with time, but does not attain room temperature at the end of the time period of observation. It appears that the temperature decreases more

rapidly for the high energy input cases, and in fact at 48 ms after the discharge, the high voltage curves appear to have a lower temperature than the low voltage curves. This temperature spread in the various voltage curves at this late time may be more of an indication of the precision of the measurements of the temperature at this time, rather than there actually being a temperature difference in those six different case. The precision of the measurements will be discussed in section 3.4.

Figure 16 shows the temperature decay with time using the same electrodes but with three different gap distances. It can be seen that the shorter the distance is, the higher is the temperature increase, as expected, because there is less gas between the electrodes to be heated. At the begining of the decay, an inverse relationship roughly exists between the temperature increase and the electrode separation. This implies that the volume of gas heated is proportional to the separation. At later times, of course, the temperature decay will depend on the initial temperature as well as heat-transfer times to the surrounding gas and the electrodes, so that an inverse relationship would not be expected to hold, which is confirmed by the curves.

The spatial variation of the temperature profiles with electrode spacing is shown in Figure 17 at two different charging voltages. The electrodes used for these measurements were the most curved of the electrodes investigated, and are labelled electrode 7; for comparison of the shape of the other

electrodes, see Figure 10b. The temperature is, as expected, greater for the smaller electrode spacings, for the same reason as given in the discussion of Figure 16.

The critical effect that the electrode shape has on the temperature profiles is indicated in Figure 18, which is a plot of the temperature increase for three electrode shapes. Qualitatively speaking, the lower the number associated with the electrode the flatter is the profile, and as indicated in Ref. [6], the more spread out is the deposited energy in the discharge. This implies that a smaller temperature increase is anticipated because the deposited energy density is lower for a flatter electrode. If we consider these temperature measurements in conjunction with the gain profiles [6] for these three electrodes, it is evident that the small-signal gain begins to saturate or decrease at the point when the input energy is sufficient to heat the gas to a temperature of approximately 450 K. Temperatures above this value indicate less than optimum conditions for maximum gain. It is not apparent whether the decrease in gain is due only to thermal effects or a decrease in pumping efficiencies; these aspects are more thoroughly discussed in Ref. [14].

Figure 19 shows the variation of temperature with position in both the horizontal (x) direction and vertical (y) direction midway between the two electrodes in the amplifier. Three different laser wavelengths were used. The time at which the temperature was measured was 3.6 ms after the discharge under the applied voltage of 50 kV. At all

positions, each measurement of temperature for the three lines were within 10 K of each other. As expected, these results show the calibration curves at each wavelength are in agreement. Similiar measurements are shown in Figure 20 under the same conditions as before but with the other gas mix. Due to the different mix, amount of deposited energy and specific heat in the discharge volume, it can be seen that the shape of the temperature profile is approximately the same but 30 K below the value of the first mix. Contrary to what we observed in 30:55:15 mix, there was no temperature rise at the region near the cathode. Further investigation is necessary to clarify this difference.

3.3 Energy Estimation

Although direct measurements of the energy deposited into the discharge were unsuccessful, this quantity can be estimated using the results presented in the previous figures. Specifically, the heat content of the gas following the discharge can be computed from the measured temperature profiles shown in Figure 12. This indicates the energy used to heat the gas only, and of course does not account for the energy emitted as radiation from the main discharge, the side sparks, or the energy present in shock and acoustic waves. The computation will be carried out under the assumption that the initial temperature distribution is constant in the y-direction, as indicated in Figure 13. Also since Figure 15 shows that the initial temperature profile is

constant for several milliseconds after the discharge, the temperature at 3.6 ms can be assumed equal to the temperature immediately after the discharge.

Assuming the gas maintains a constant pressure and that the heat energy density ϵ is a function of x only, then $\epsilon(x)$ is given by

$$\epsilon(x) = \int_{T_o}^{T_i(x)} \rho(T) C_p(T) dT \qquad (2)$$

where ρ, C_p, T_i and T_o are the gas density, specific heat at constant pressure, the gas temperature immediately following the discharge, and room temperature, respectively. Values for $T_i(x)$ can be obtained from Figure 12.

For the gas mixture, C_p was calculated following Cloutier [41] using appropriate tables from Hamblin [42]. In table 2, $\epsilon(x)$ was calculated from eq. (2) using Simpson's rule for numerical integration. Integration* of $\epsilon(x)$ throughout the volume of the discharge then gives the total heat energy of the gas. An example is shown below for conditions indicated in Figure 12 for V= 50 kV, where the temperature distribution curve has been extrapolated to room temperature at both ends.

---

* numerical integration

Table 2 Details of Energy Estimation for Input Voltage= 50 kV.

x (cm)	$T_i(x)$ (K)	$\epsilon(x)$ (J/cm^3)
-3.06	312	0.0165
-2.55	360	0.0562
-2.04	400	0.0830
-1.53	440	0.1058
-1.02	470	0.1209
-0.51	495	0.1323
0.00	505	0.1366
0.51	500	0.1344
1.02	480	0.1260
1.53	460	0.1160
2.04	425	0.0977
2.55	395	0.0799
3.06	356	0.0532
3.57	312	0.0165

Then the total heat energy E in the gas is given by

$$E = \iiint \epsilon(x)\,dx\,dy\,dz = \left[\int_x \epsilon(x)\,dx\right] YZ$$

Where Y= the depth of the discharge volume in the y direction= 5.08 cm

Z= the length of the discharge volume in the z direction= 51.4 cm

$$E = \left[\int_{-3.06}^{3.57} \epsilon(x)\,dx\right] \times 5.08 \times 51.4$$

$$= 186.6 \text{ Joules}$$

The total applied energy $= 2(\frac{1}{2} CV^2)$

$$= 0.1 \times 10^{-6} \times (50 \times 10^3)^2$$

$$= 250 \text{ Joules}$$

Percentage of the deposited energy $= \dfrac{186.6}{250} = 74.6\ \%$

For the six voltages indicated in Figure 12, using these temperature distribution curves extrapolated at the edges to room temperature, the heat energy is found to be equal approximately to 75% of the energy initially placed on the capacitors. The results for all voltages are summarized in Table 3. Thus, irrespective of the charging voltage, 75% of the electrical energy goes into heating the gas.

Table 3 Summary of the Percentage of the Deposited Energy for the Input Voltage from 35 to 60 kV.

Input Voltage(kV)	Input Energy(J)	Deposited Energy(J)	Percentage (%)
35	122.5	92.1	75.2
40	160.0	120.0	75.0
45	202.5	152.0	75.0
50	250.0	186.6	74.6
55	302.5	226.3	74.8
60	360.0	268.0	74.4

3.4 Errors

In Chapter 2, we have shown that the transmission β through an absorbing gas is given by

$$\beta = \frac{I}{I_o} = \exp(-kL) \qquad (3)$$

where I_o is the input intensity and I is the intensity at a distance L in the absorber. Taking differentials and re-arranging, we get

$$\frac{\Delta k}{k} = -\left(\frac{1}{\ln \beta^{-1}} \frac{\Delta \beta}{\beta} + \frac{\Delta L}{L} \right) \qquad (4)$$

where Δk, $\Delta \beta$ and ΔL can represent the errors in the absorption coefficient, transmission and length, respetively.

Following the method of Dorn and McCracken [15], and if no systematic errors are present, the upper bound on the relative error in k, γ_k, can be written as

$$| \gamma_k | \leq \left(\frac{1}{\ln \beta^{-1}} \right) | \gamma_\beta | + | \gamma_L | \qquad (5)$$

where γ_β and γ_L are the relative errors in β and L, respectively.

When $\beta \approx 1$, the first term in eq. (5), containing $1/\ln \beta^{-1}$, will present the dominating effect in determining the upper bound on the error because of the characteristics of the logarithmic function. If a high precision in k is desired, β must be measured precisely.

In the auxiliary experiment, β is calculated from the ratio of two digital-volmeter readings, and the maximum relative error in β is estimated at ±5%. The length of the absorption cell is known much more accurately and its contribution in eq. (5) is negligible. Using eq. (5), the bounds on the error in k varied from 60% at 310 K to 6.5% at 580 K for the 30:55:15 mix; the absolute errors were approximately equal to $\pm 0.6 \times 10^{-3} cm^{-1}$ at all temperatures and are indicated in Figure 5. For pure CO_2, the bounds on the error in k varied from 30% at 300 K to 2.5% at 600 K; the absolute errors were approximately equal to $\pm 0.4 \times 10^{-3}$ cm^{-1} at all temperatures and are indicated in Figure 4.

Similiar error bounds were found for 13:77:10, and are indicated in Figure 6.

In the temperature experiment, the precision is not as good because the length of the absorber (ie. the heated gas between the electrodes) is not known as accurately and the uncertainty in length is estimated to be about ±5%. Also, since the absorber is shorter, the transmissions are larger, and hence the $1/\ln \beta^{-1}$ factor is greater. Again assuming a ±5% estimation in β, a bound on the error may be obtained using eq. (5) and Figure 5. The bound of the temperature varies approximately from ±20 K at 300 K to ±30 K at 600 K.

Due to the length of time required to perform the temperature measurement, it was not feasible to repeat experiments to obtain data under all conditions to obtain a precise standard deviation. However, as the results show from Figures 19 and 20, the temperature was always computed to be within 10 K in each case when the temperature measurement was performed at three different wavelengths for the two different mixes. Thus, the bound on the error quoted above is felt to be a realistic one.

3.5 Correction of Temperature Measurement

The ratio of the amplitudes of the absorbed and the non-absorbed traces does not represent the real transmission through the gas mix in the amplifier; a correction factor to the absorption coefficient at room temperature has to

be considered. In what follows, we will show how to find the true absorption coefficient.

Consider the following system:

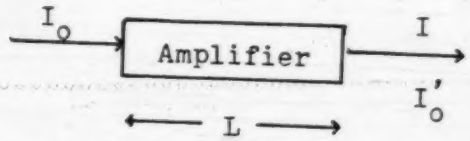

I_o = Intensity of beam before entering the amplifier

I_o' = Intensity of beam out of the amplifier, without discharge

I = Intensity of beam out of the amplifier, with discharge

At room temperature ($T_o \approx 300$ K),

$$I_o' = I_o \exp [-k(T_o)L]$$

After the discharge, the intensity will be

$$I = I_o \exp [-k(T) L]$$

Then the apparent transmission is

$$\beta' = \frac{I}{I_o} = \exp - [k(T) - k(T_o)] L$$

$$k(T) - k(T_o) = \frac{1}{L} \ln (\beta')^{-1}$$

$$k(T) = k(T_o) + \frac{1}{L} \ln (\beta')^{-1}$$

This shows that the true value of absorption coefficient will be equal to the value at room temperature added to the apparent absorption coefficient obtained from the photographs.

CHAPTER 4

CONCLUSIONS AND SUGGESTIONS FOR FURTHER RESEARCH

4.1 Summary of Results and Conclusions

The effects of gas temperature and the importance of controlling gas temperature in a TEA CO_2 laser have been outlined in the introduction. Laser devices, both in single pulsed discharges and high-repetition-rate discharges, must be designed to operate at an optimum temperature for maximum laser output or amplification.

In Chapter 2, measurements of the absorption coefficient as a function of temperature for pure CO_2 and two other gas mixes have been described. It was found that the P(20) absorption coefficient did not vary with pressure over a range from 100 to 700 torr in pure CO_2 at high temperature, within the precision of the measurement. A consideration of the contribution from the mixed mode absorption, proposed by Munjee and Christensen, cannot explain the descrepancy between the theoretical calculation and the experimental measurement because their calculations predict a 28% variation of the absorption coefficient as the pressure goes from 100 to 700 torr at a temperature of 500 K. In the pure CO_2 case the agreement between the results and those of Leonard are satisfactory except the spread of his values at high temperature. These indicate that this auxiliary experiment is necessary and its data can be used subsequently for the measurement of

equilibrium temperature in a TEA CO_2 laser amplifier.

In Chapter 3, a method of measuring the equilibrium gas temperature in a TEA CO_2 laser amplifier following the discharge has been described by considering the absorption suffered by a CO_2 laser beam. Using electrodes with Chang profiles, temperatures as high as 600±30 K were observed at the center of the discharge. The results show that the temperature decreases in an approximately symmetric fashion towards the edges. A constant temperature distribution along the main current flowing in the discharge was also found. The temperature behaved as expected with respect to the other parameters; it increased with input energy and decreased with pressure, electrode spacing, and curvature of electrode profile. It was found that the gas cooled down to room temperature in more than 50 ms.

For the system used here and for the particular gas mix employed, the maximum small-signal gain occurs at a temperature of approximately 450 K obtained by considering the temperature profiles in conjunction with the gain profiles [6]. A temperature above this value indicates less than optimum conditions for maximum gain.

4.2 Suggestions for Further Research

As far as the spatial resolution of the temperature profile is concerned, the temperature rise in the region near the electrodes should be investigated further. This is necessary for the following resons: (1) to ascertain whether

there is a temperature rise in one mix (30:55:15) but not in the other (13:77:10); (2) to find more exactly the behavior of the temperature gradient near each electrode. One way of obtaining better resolution of the temperature profile is to reduce the diameter of the iris and put it closer to the amplifier. Further, in order to eliminate possible spurious readings due to reflection of the laser beam from the electrodes, another iris should be placed in front of detector system. For convenience, the iris, the focal lens and the detector could be placed in fixed relative positions in one unit. We would expect a temperature drop near both electrodes; with sufficient spatial resolution, this drop in temperature will be measurable. Moreover, an accurate temperature profile along the y-direction will provide data for a theoretical temperature model, as discussed below.

From the viewpoint of temperature control, it is necessary to know the temperature decay at many more points between the electrodes than those investigated. As can be seen, to perform an entire set of measurements would be very time consuming and expensive. Therefore, it is desirable to develop a theoretical model of temperature with both temporal and spatial resolution. This model would enable us to perdict the temperature profile in different gas-mix systems without making a large number of tedious measurements. The model might be obtained by numerically solving a three-dimensional heat conduction equation, in conjuction with the continuity equation, provided sufficient data and the initial

conditions are available. Since the absorption coefficient was assumed to be constant along the z-direction, it would be appropriate to begin by solving the two-dimensional heat equation first. The validity of such a model should be tested by comparing the predicted and measured temperature decay at specific positions. If agreement is not obtained, further refinement of the model would be necessary. This would require the solution of a three-dimensional heat equation.

The model discussed in the previous section was restricted to a single pulse discharge system with very slow gas flow. In high-repetition-rate discharge systems, a similar model can be found by numerically solving the heat and mass-balance equations. We would expect that the temperature decay to be faster upstream. Also by increasing the gas flow rate and pulse rate gradually, we could measure the temperature decay at certain positions between the electrodes. It would be interesting to compare the predicted temperature decay from the model with that measured. If there is correspondence between the two, the design and construction of gas circulating and cooling systems would be made easier since the model could then be used to predict the temperature relaxation time.

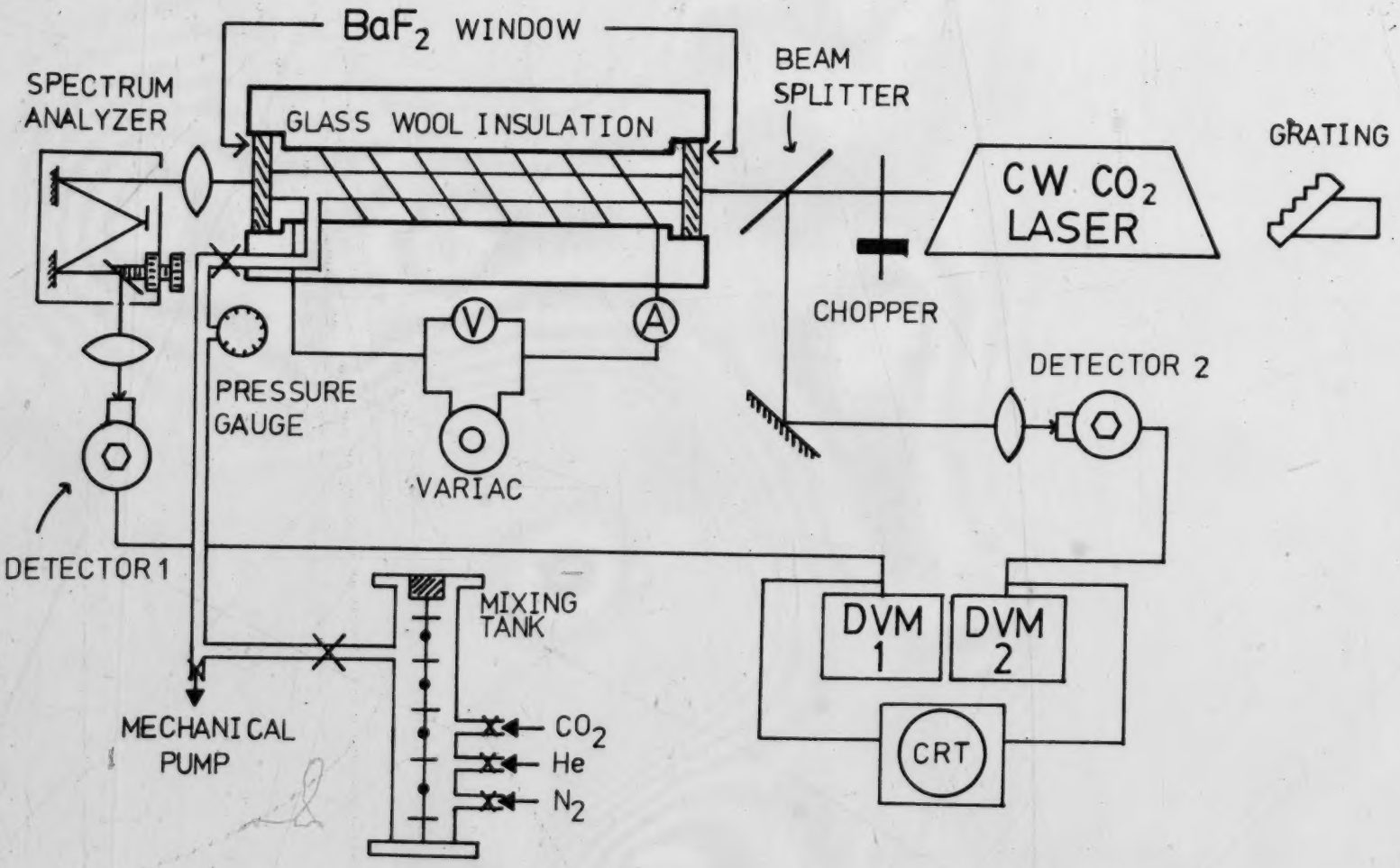

FIGURE 1. Schematic diagram of absorption measurement configuration.

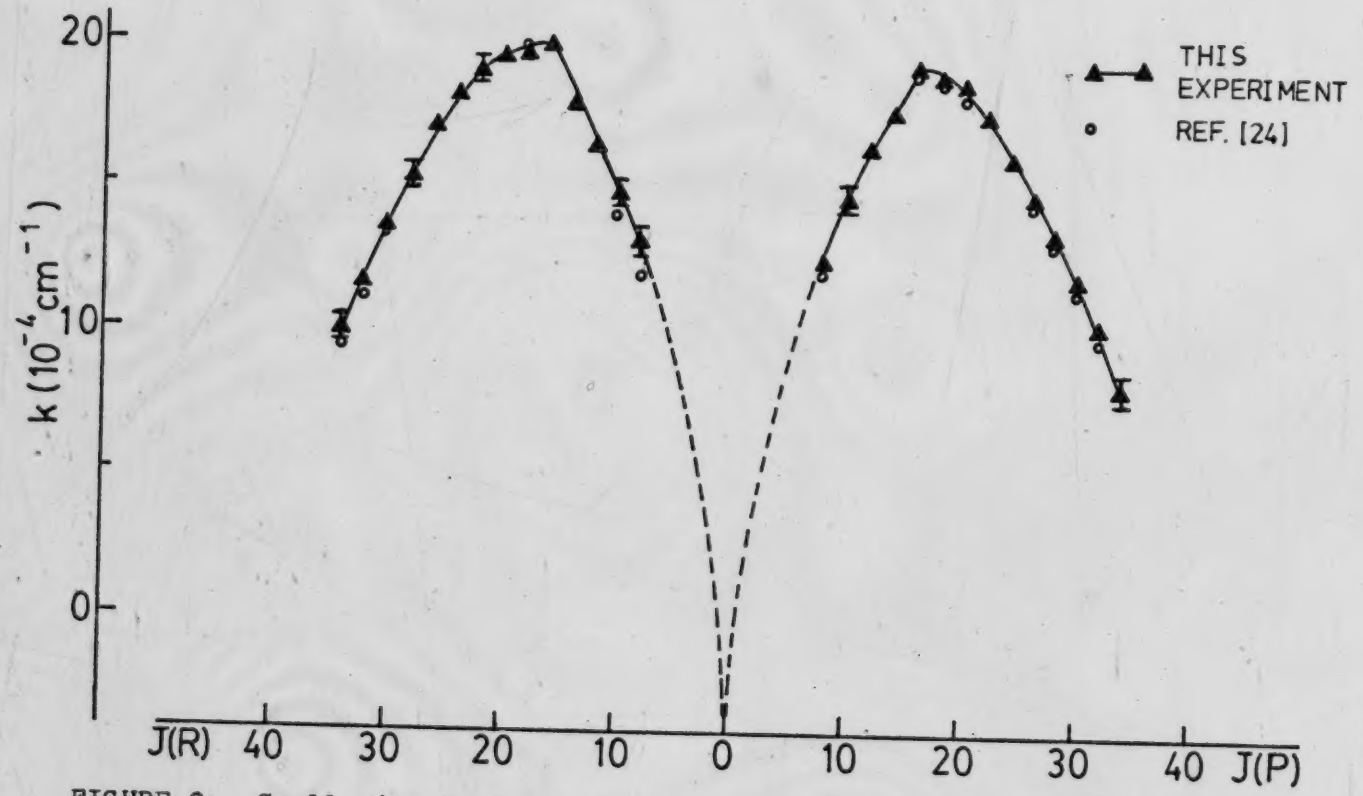

FIGURE 2. Small signal absorption coefficient of various R and P branch CO_2 laser transitions in the 10.6 μm band at 310 K in 100:0:0 mix.

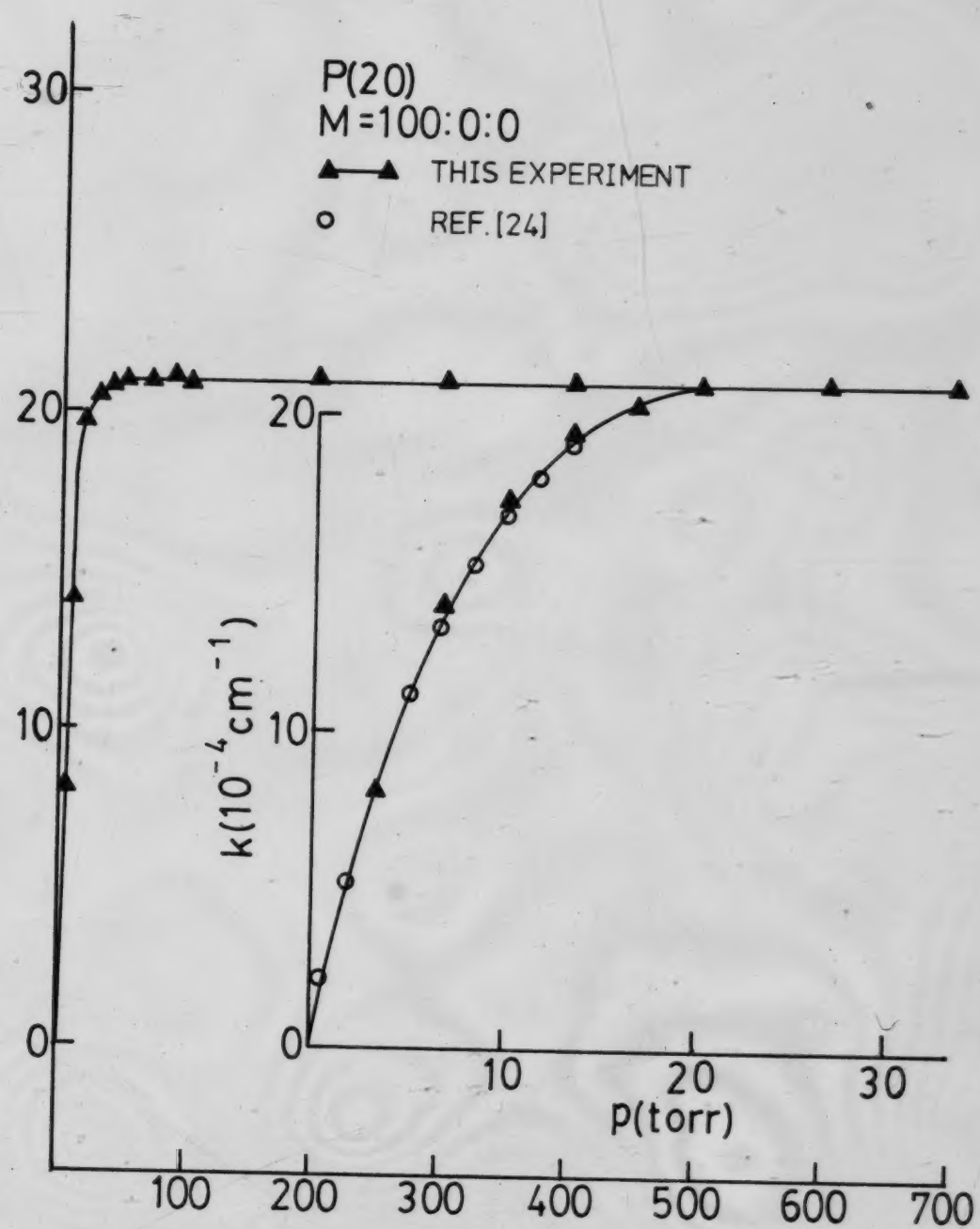

FIGURE 3. Small signal absorption coefficient at various pressures for P(20) at 310 K and M=100:0:0.

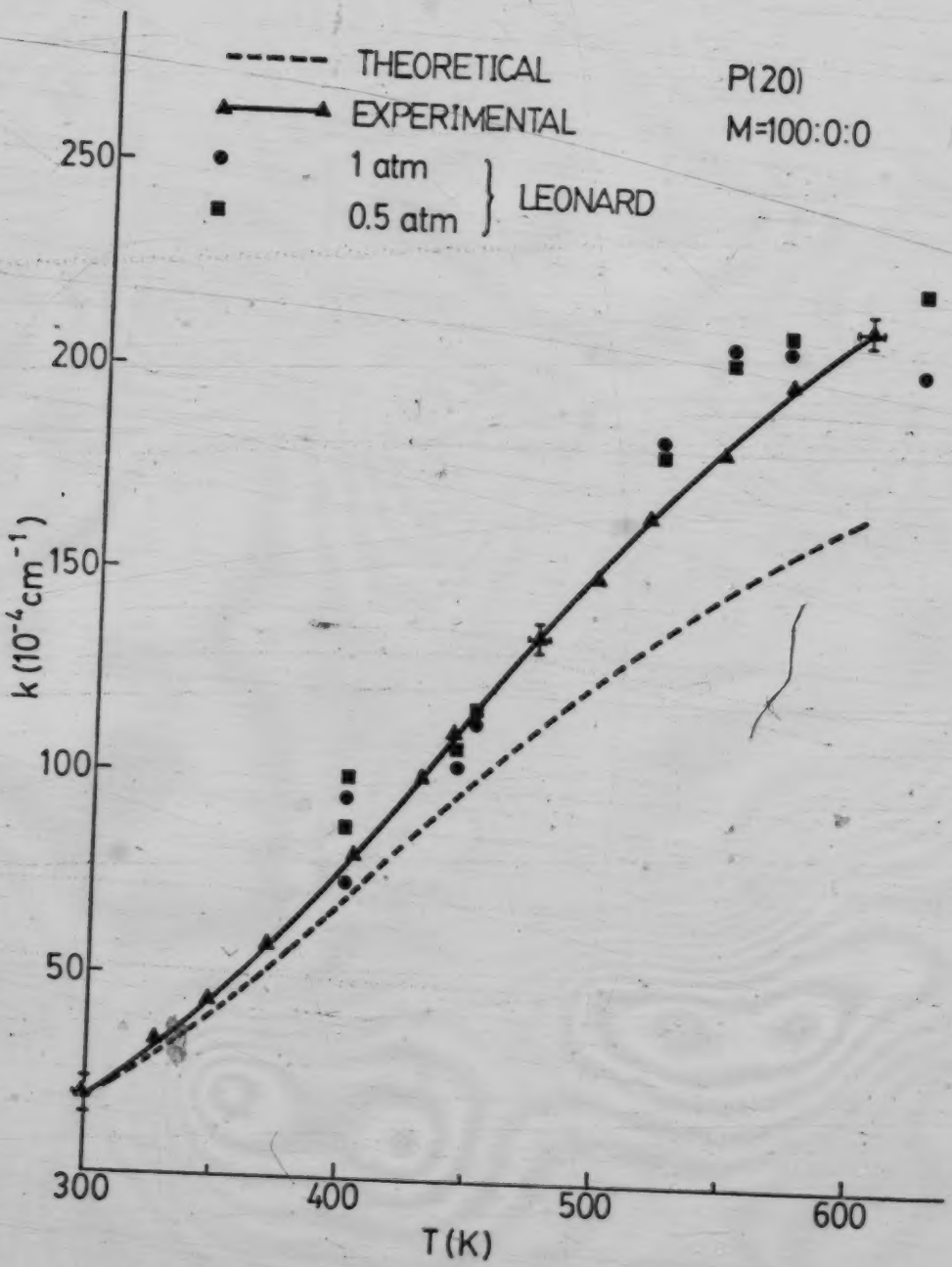

FIGURE 4. Absorption coefficient as a function of temperature for P(20) in pure CO_2 (M=100:0:0).

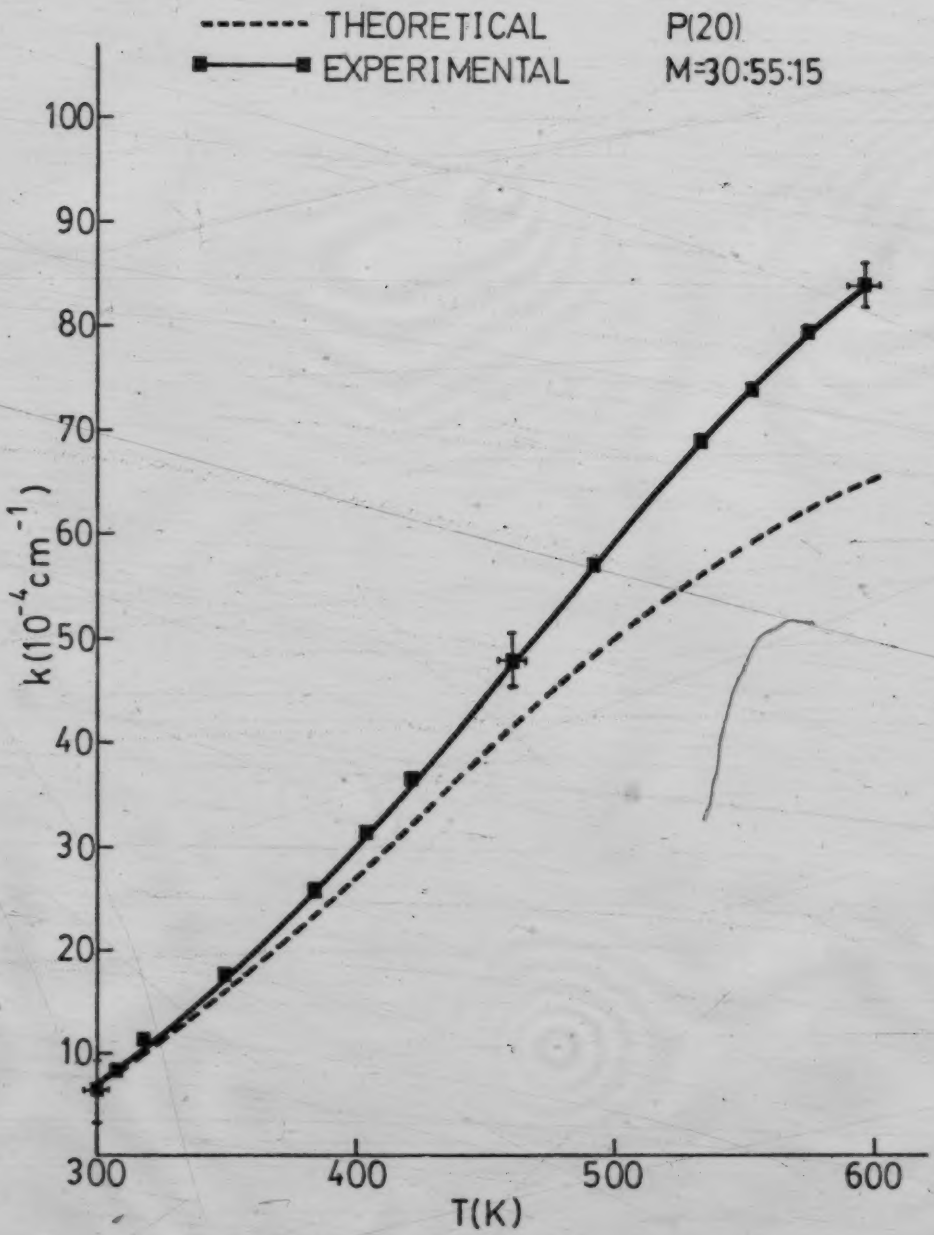

FIGURE 5. Absorption coefficient as a function of temperature for P(20) in gas mix(M=30:55:15).

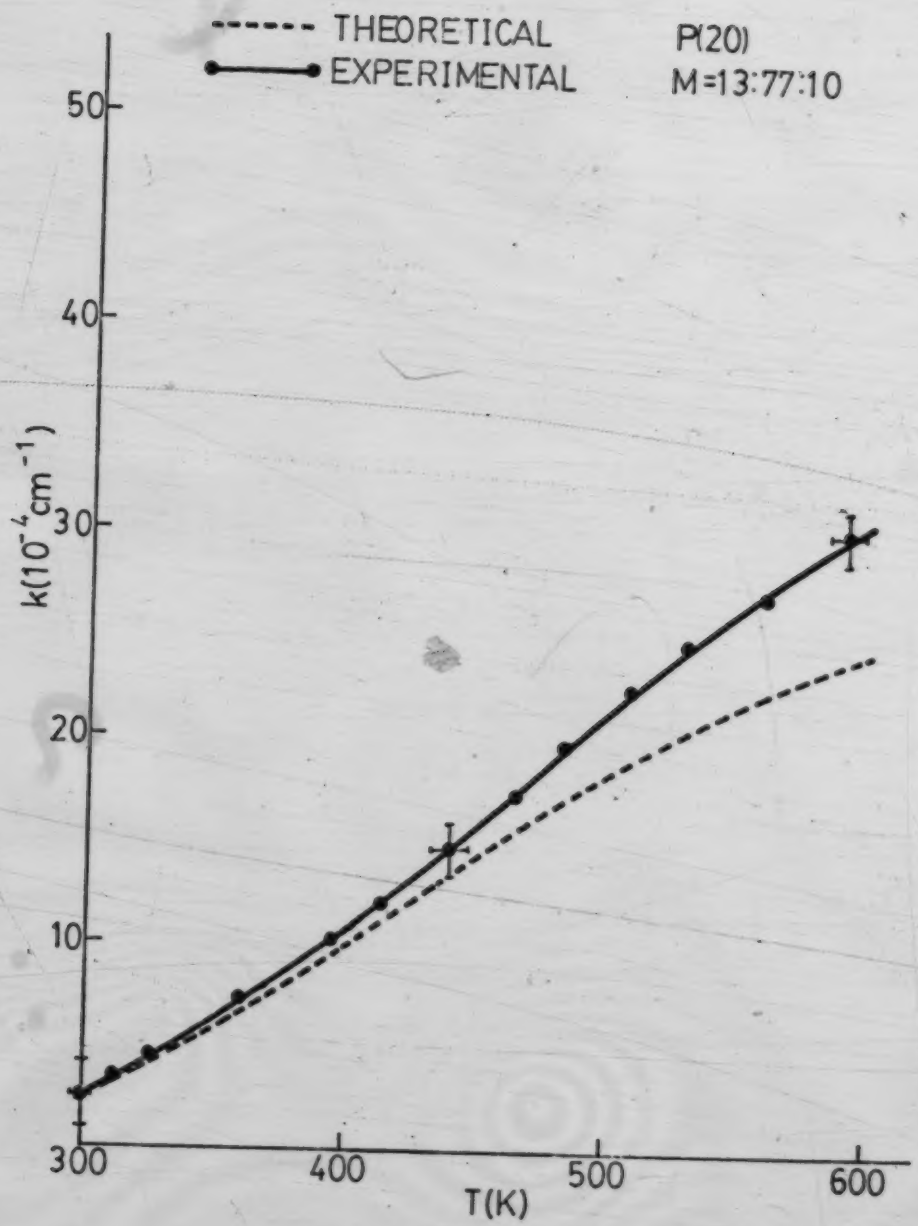

FIGURE 6. Absorption coefficient as a function of temperature for P(20) in gas mix(M=13:77:10).

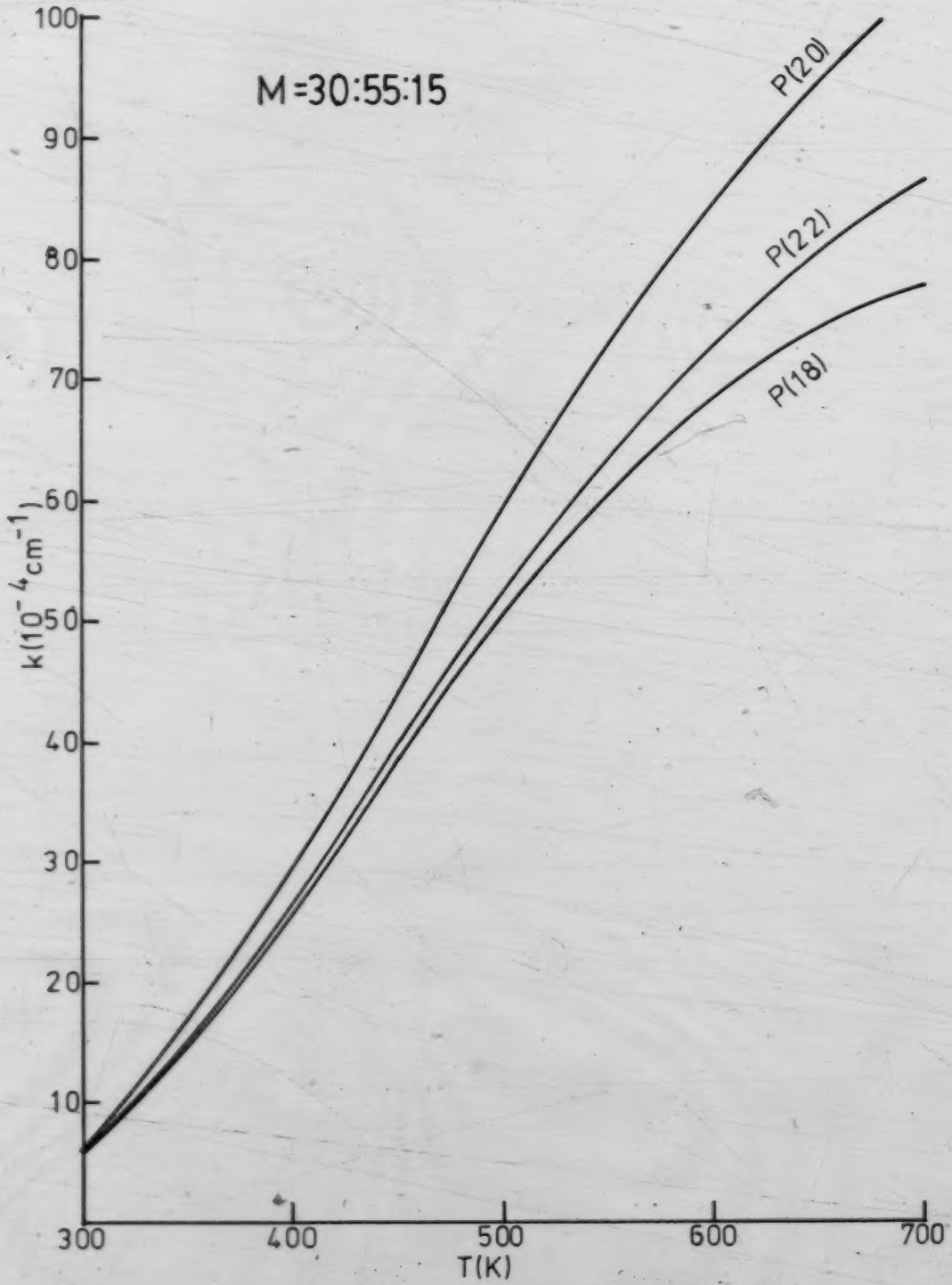

FIGURE 7. Standard curve of absorption coefficient against temperature for P(20), P(22), P(18) at M=30:55:15.

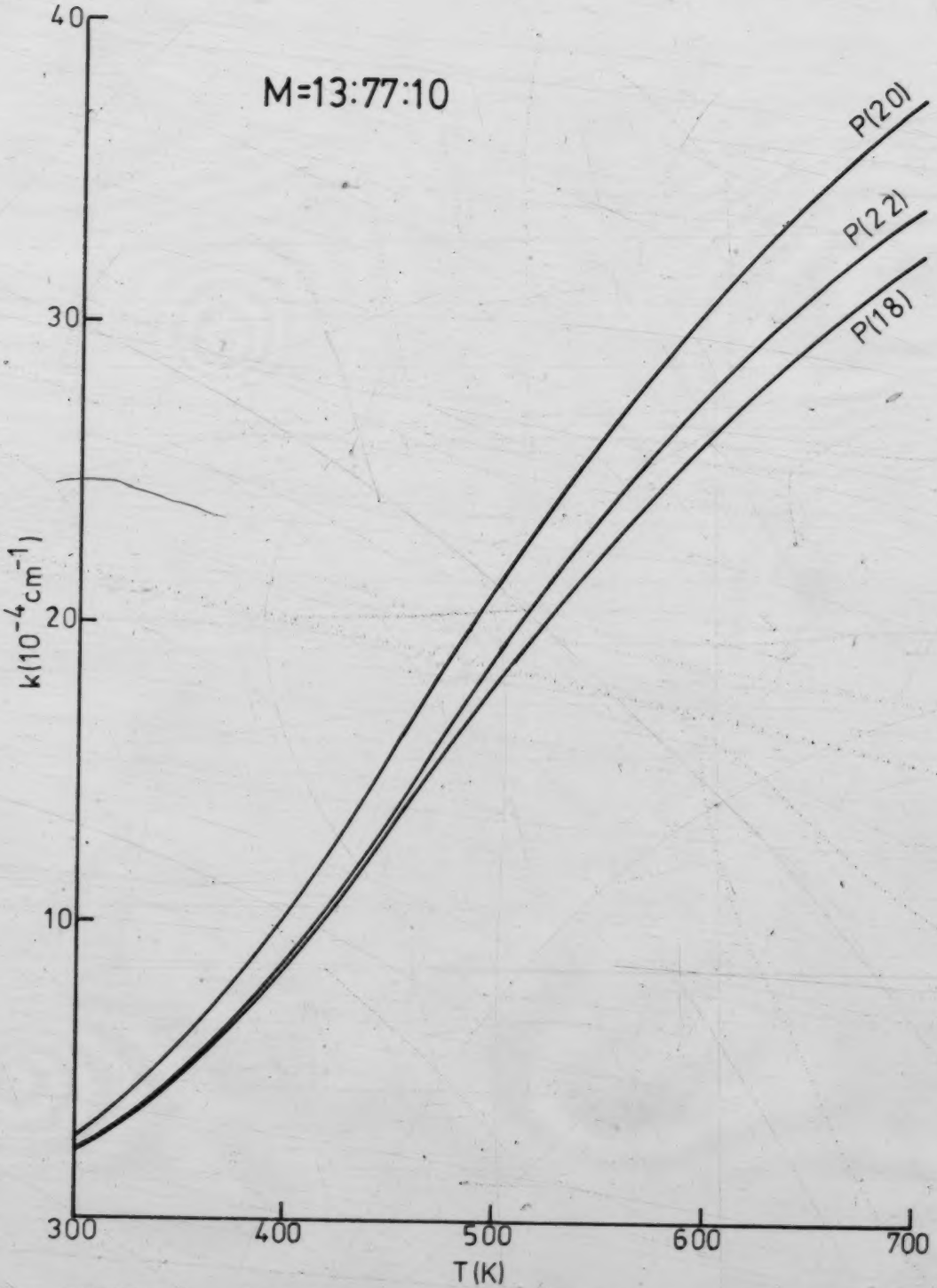

FIGURE 8. Standard curve of absorption coefficient against temperature for P(20), P(22), P(18) at M=10:77:13.

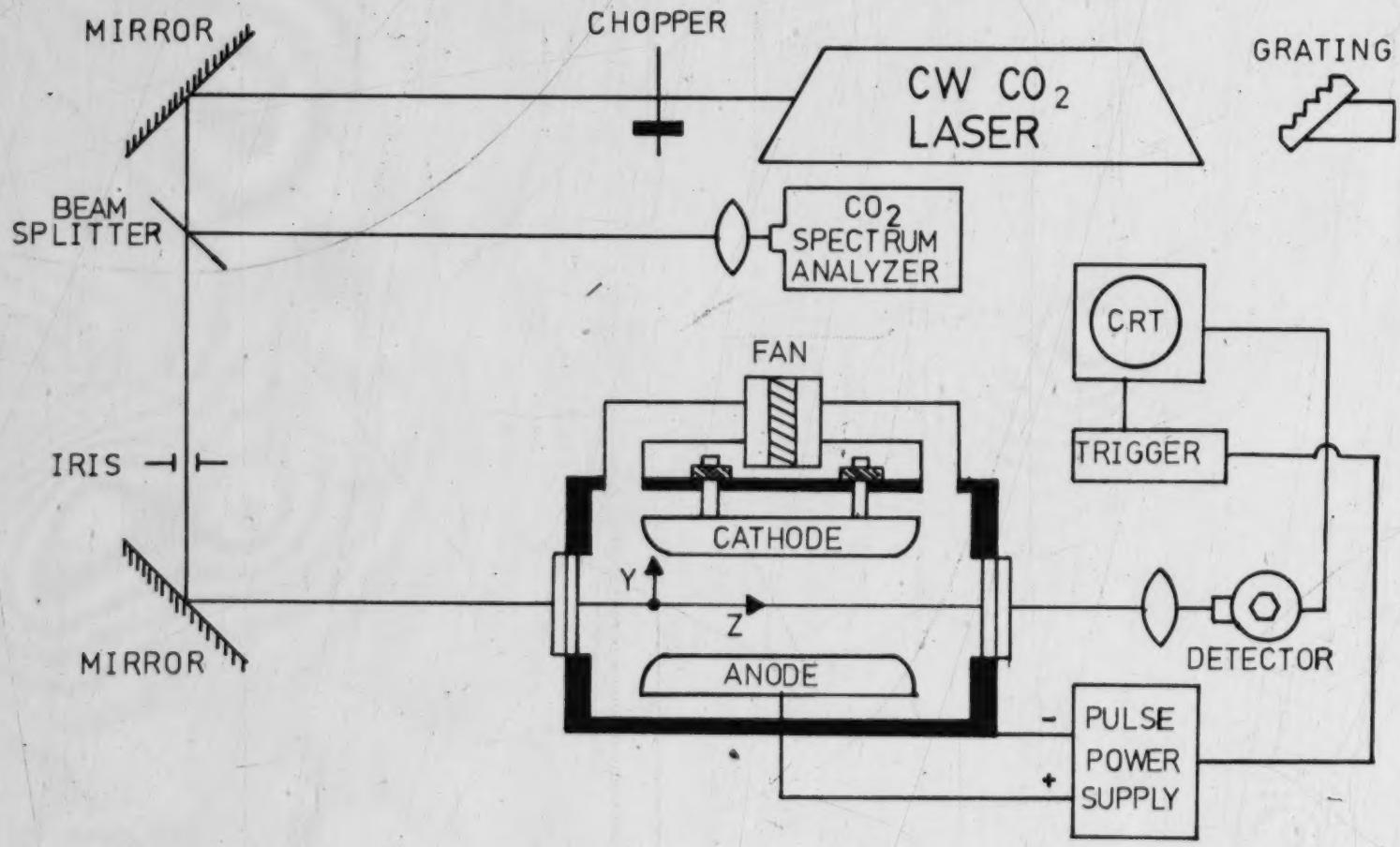

FIGURE 9. Schematic diagram of temperature measurement configuration.

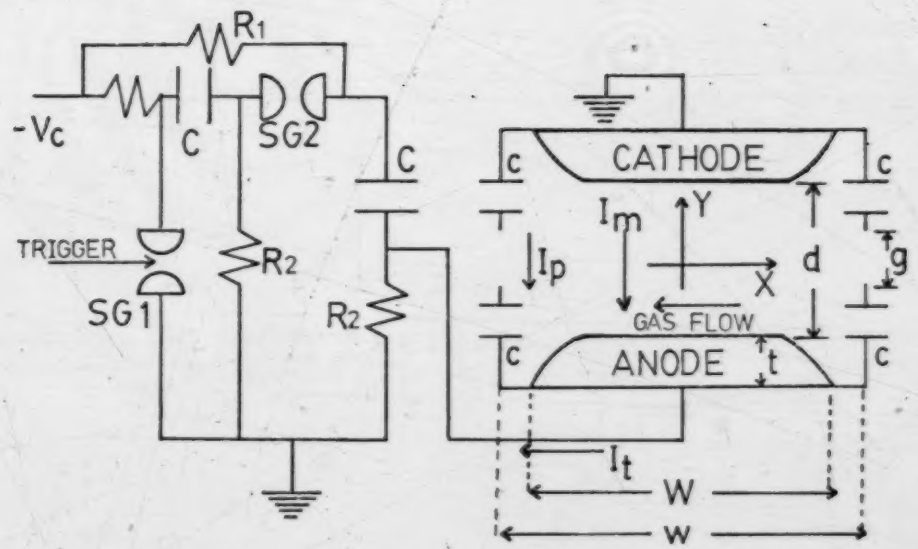

FIGURE 10a. Amplifier and discharge circuit diagram.

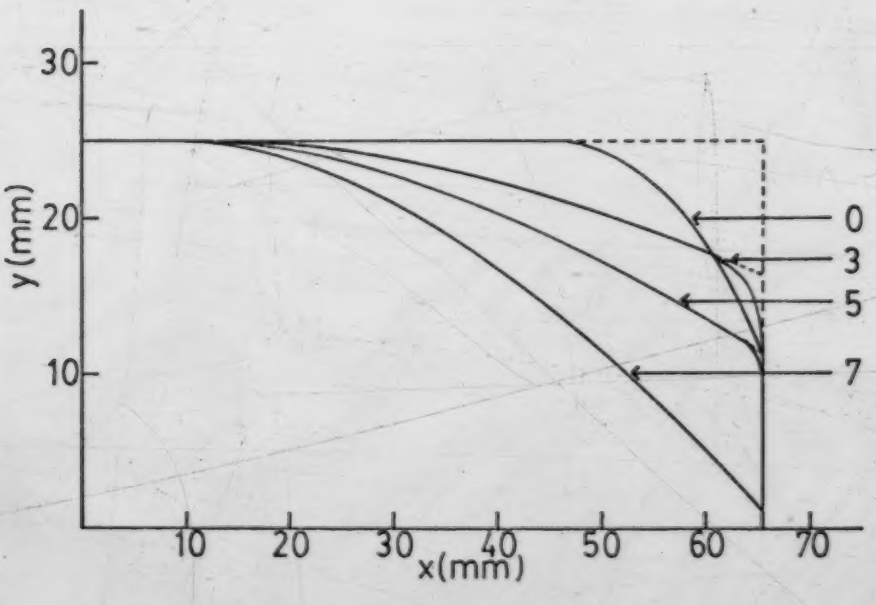

FIGURE 10b. Cross section of four electrode shapes.

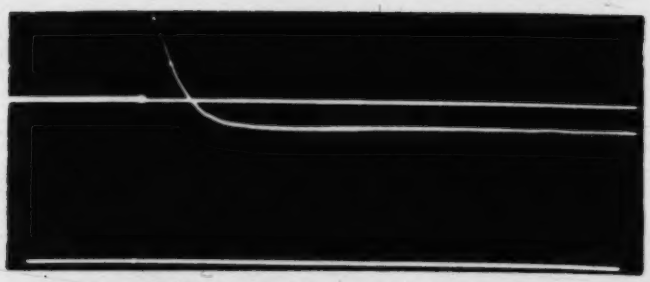

a. 20 μs/cm

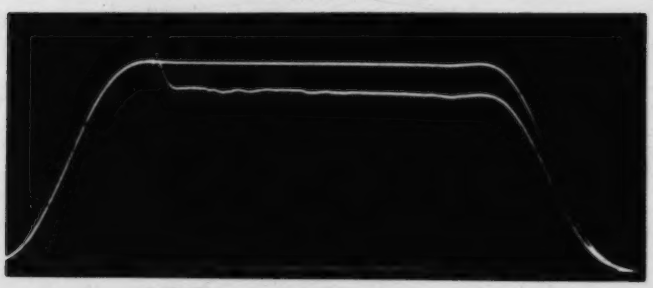

b. 200 μs/cm

c. 1000 μs/cm

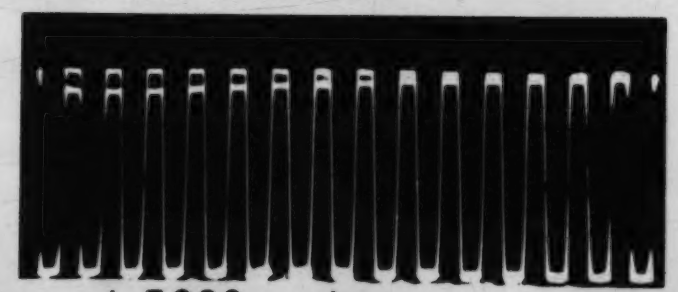

d. 5000 μs/cm

FIGURE 11. Oscilloscope traces of temperature measurement.

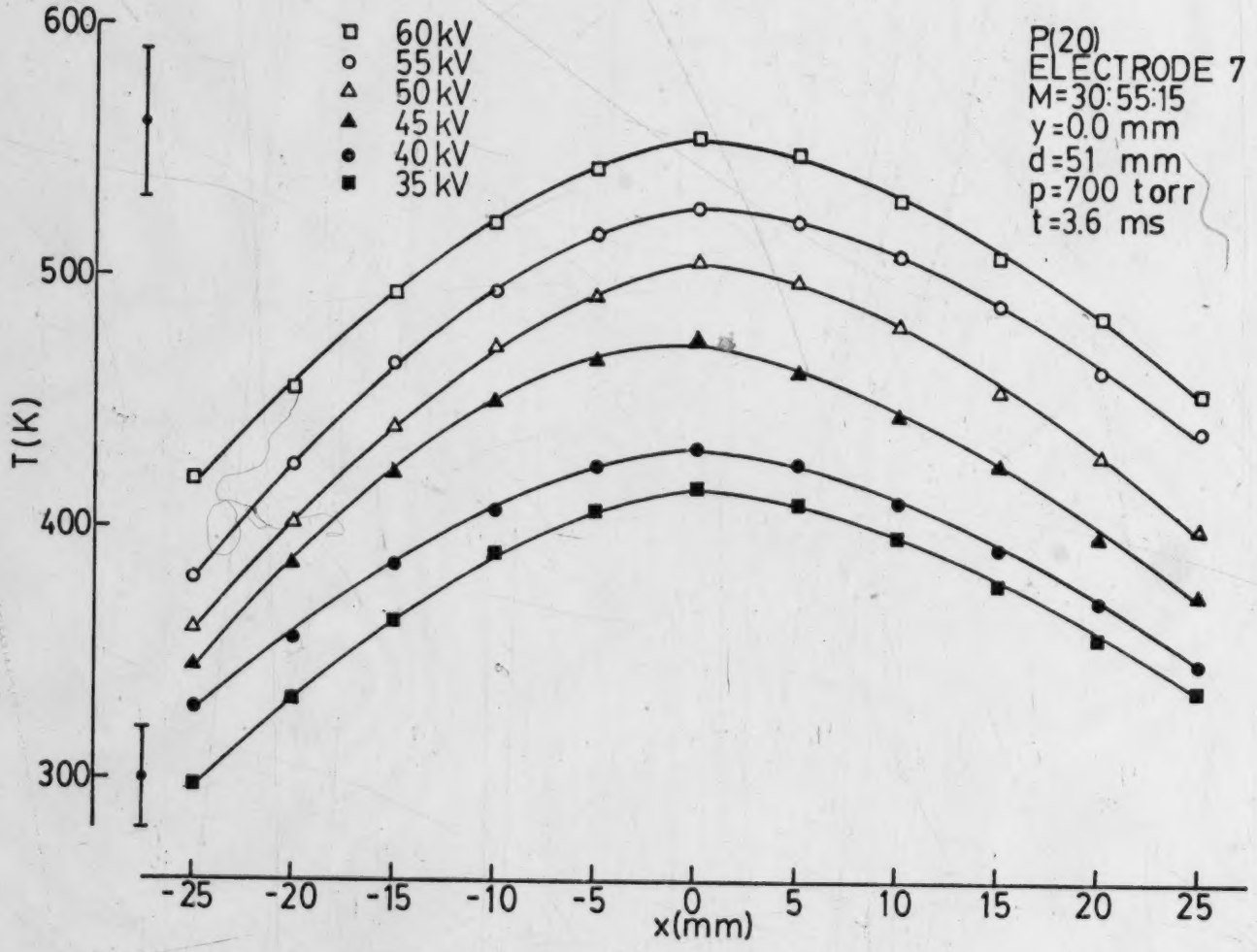

FIGURE 12. Temperature profile with x position.

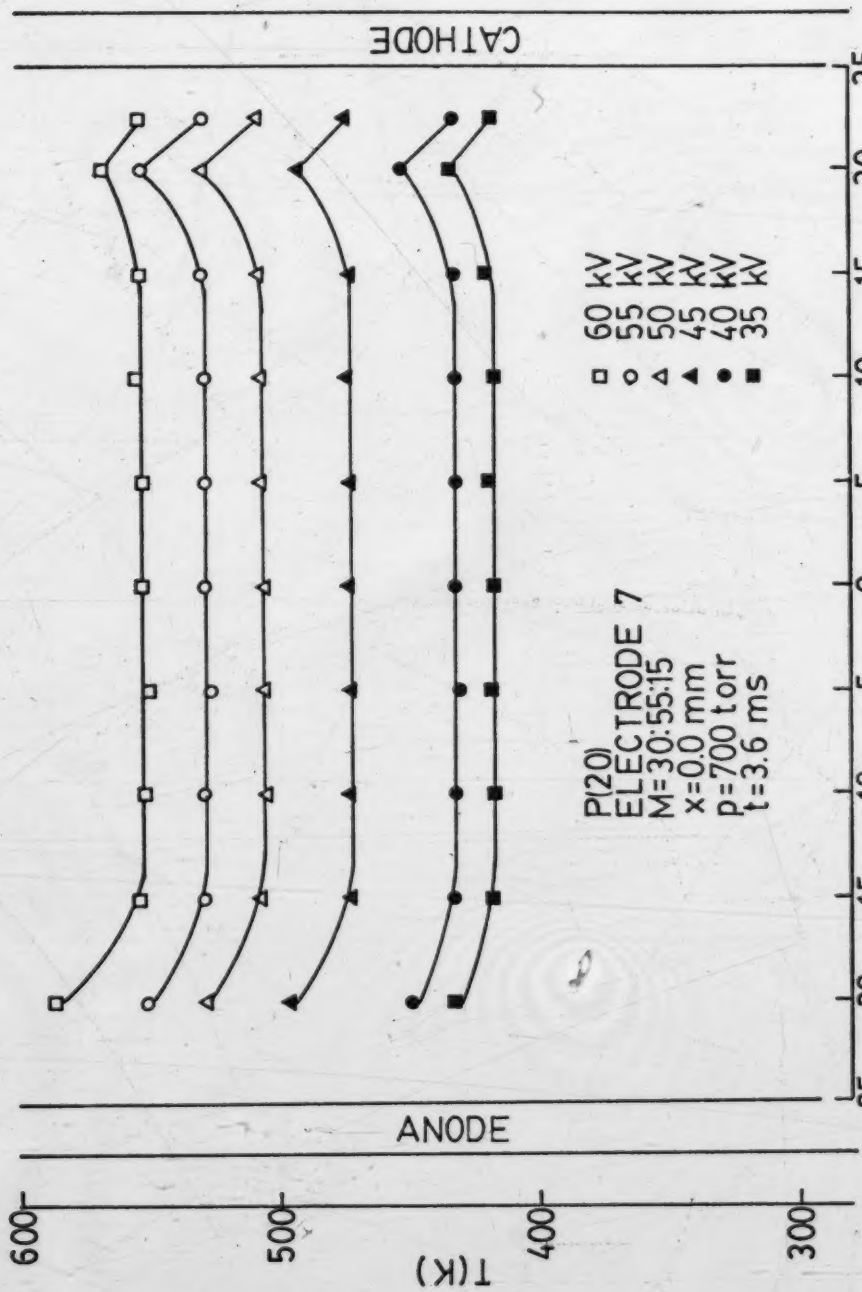

FIGURE 13. Temperature profile with y position.

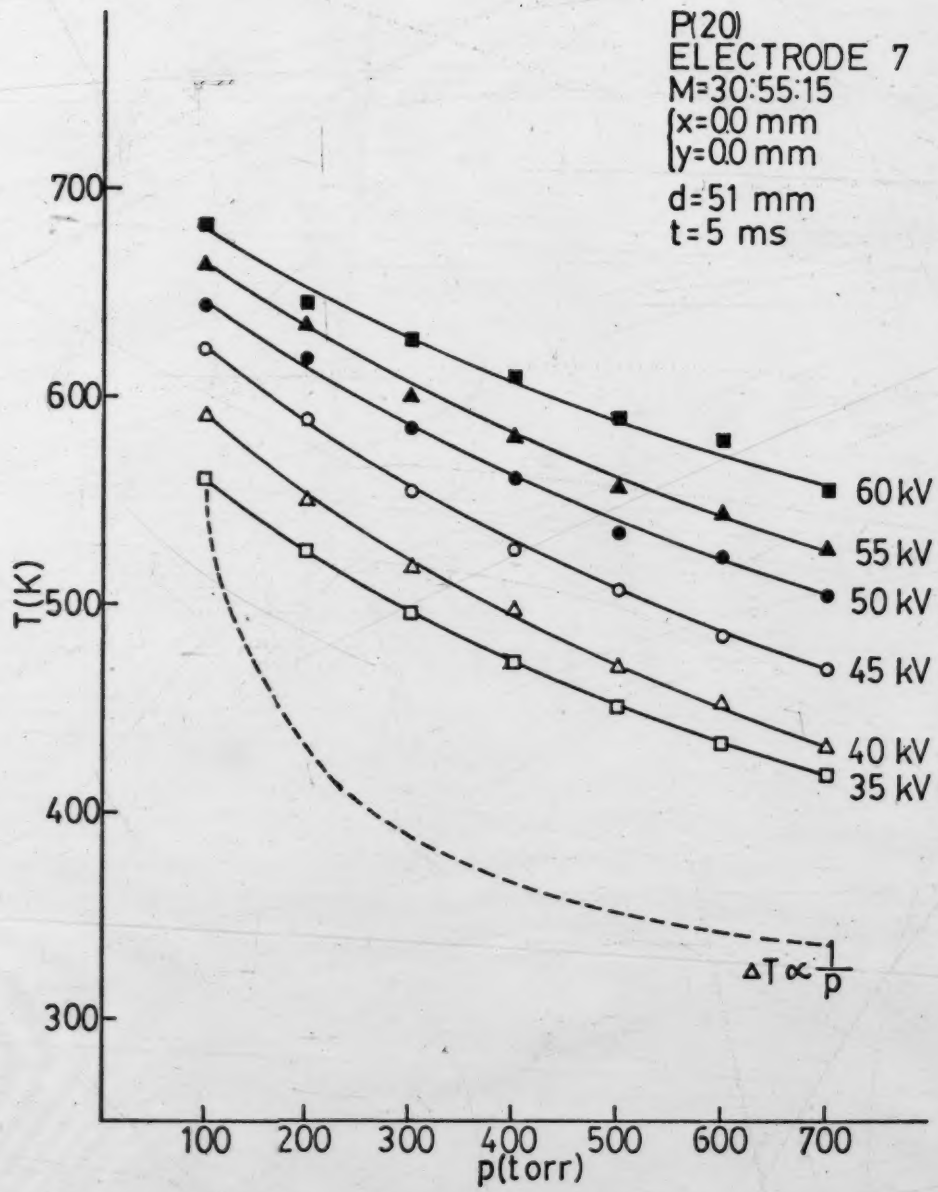

FIGURE 14. Temperature profile with pressure.

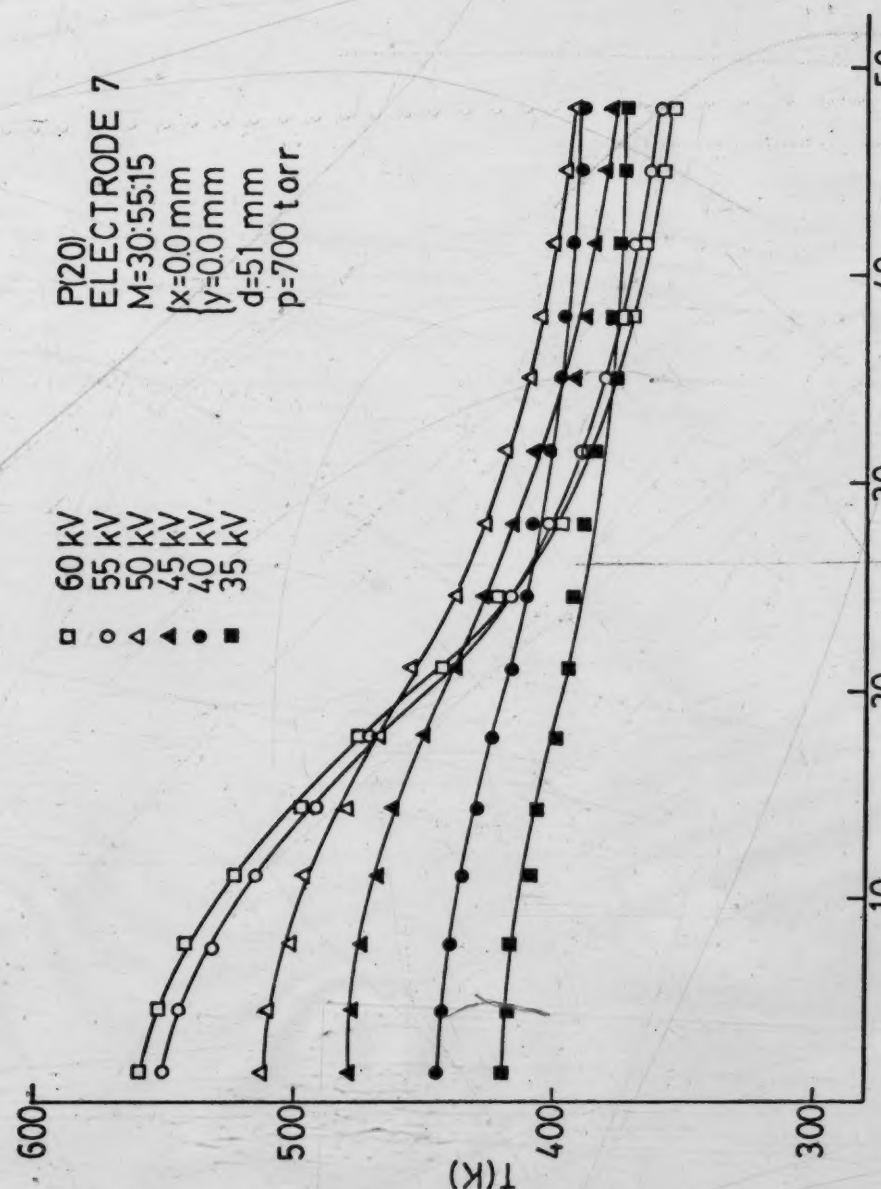

FIGURE 15. Temperature decay with time.

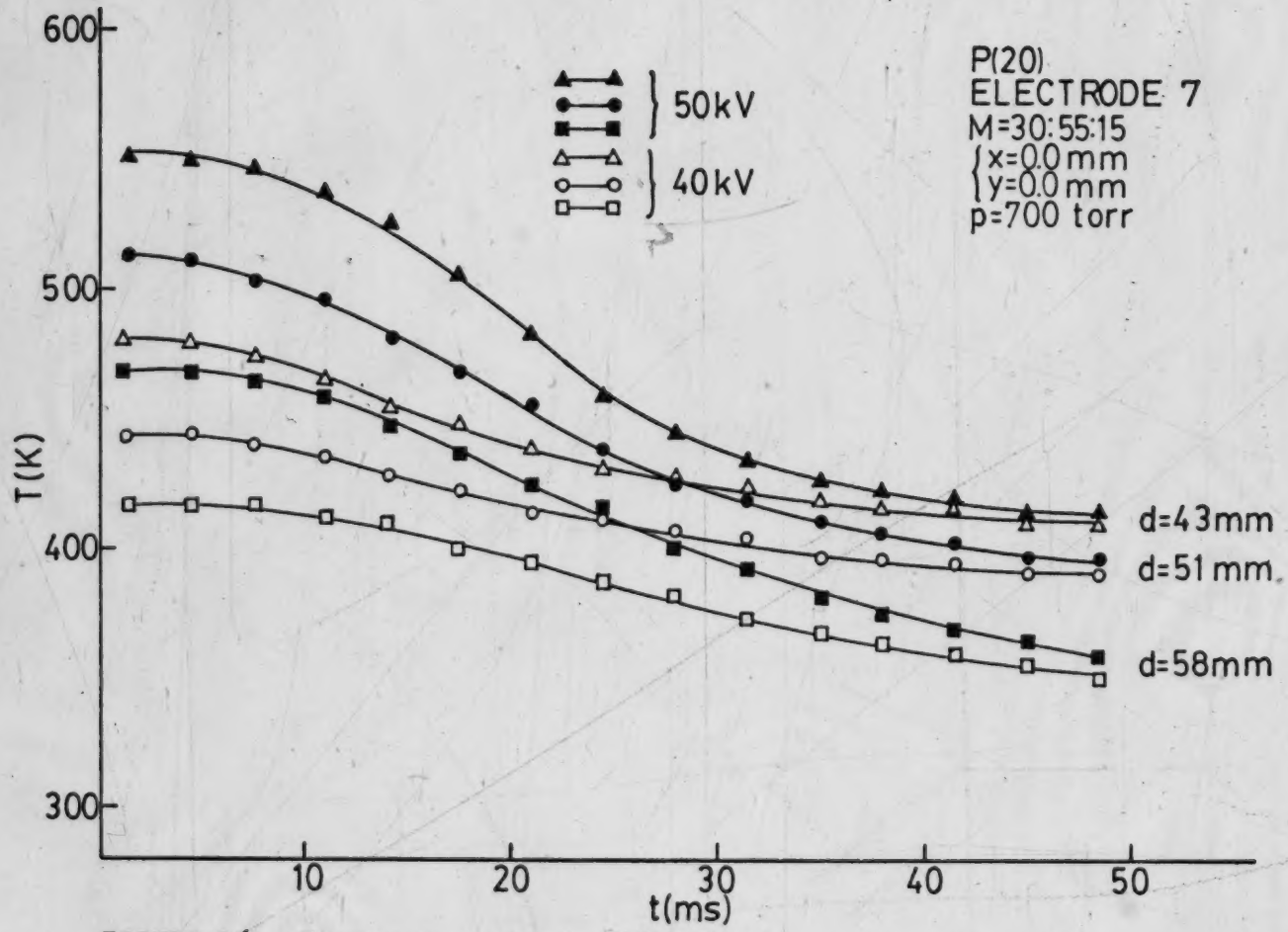

FIGURE 16. Temperature decay with time.

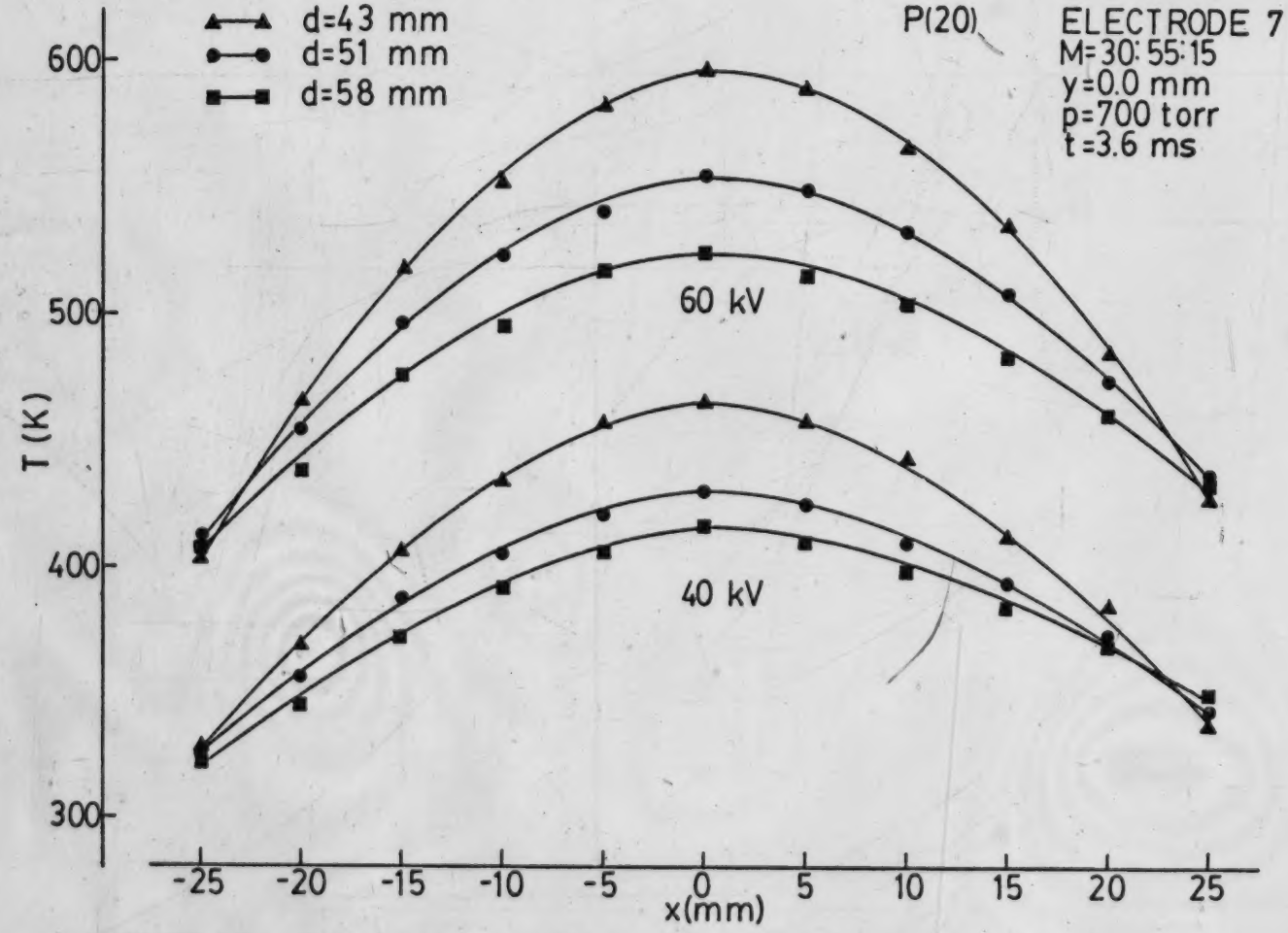

FIGURE 17. Temperature profile with x position.

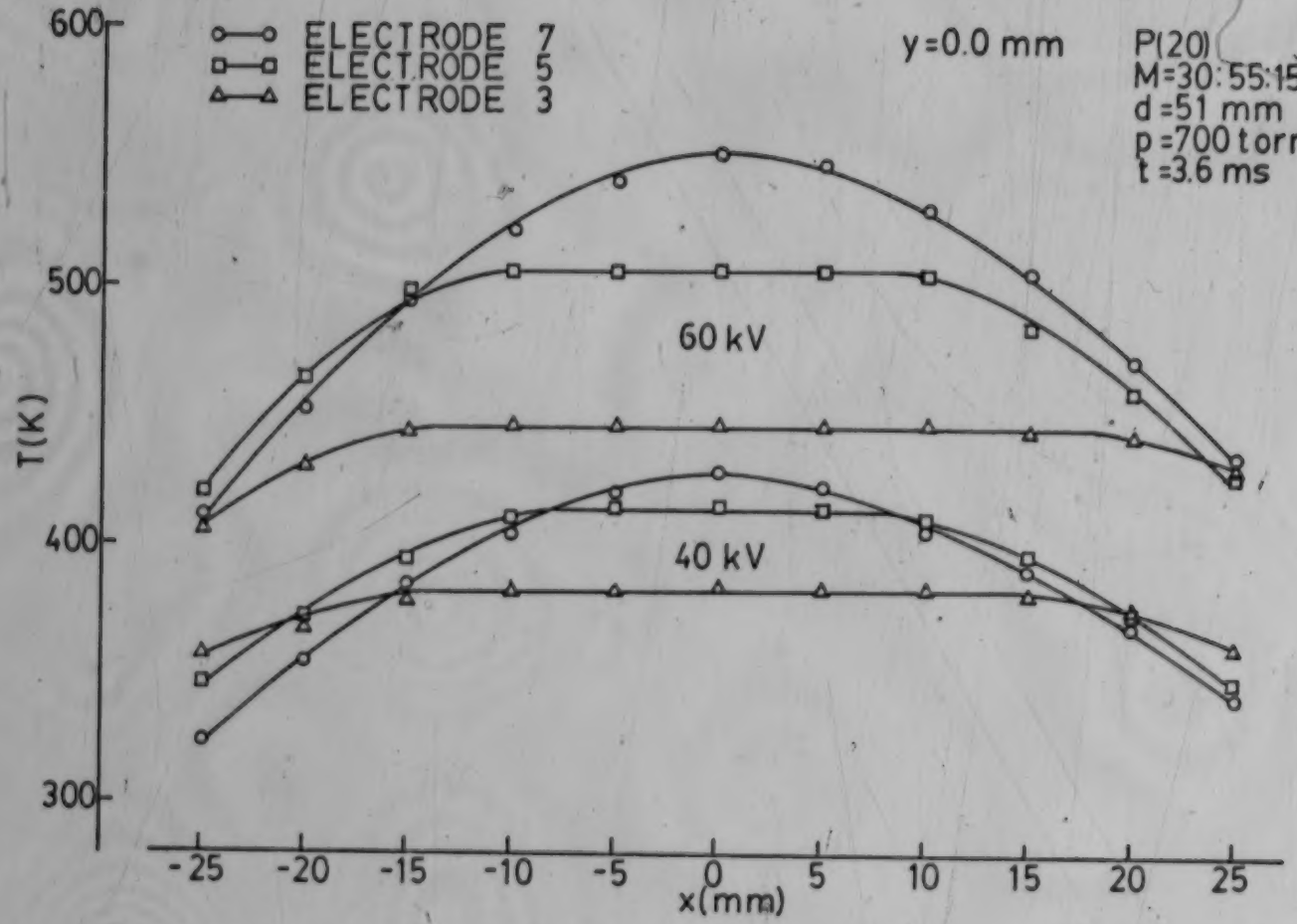

FIGURE 18. Temperature profile with x position.

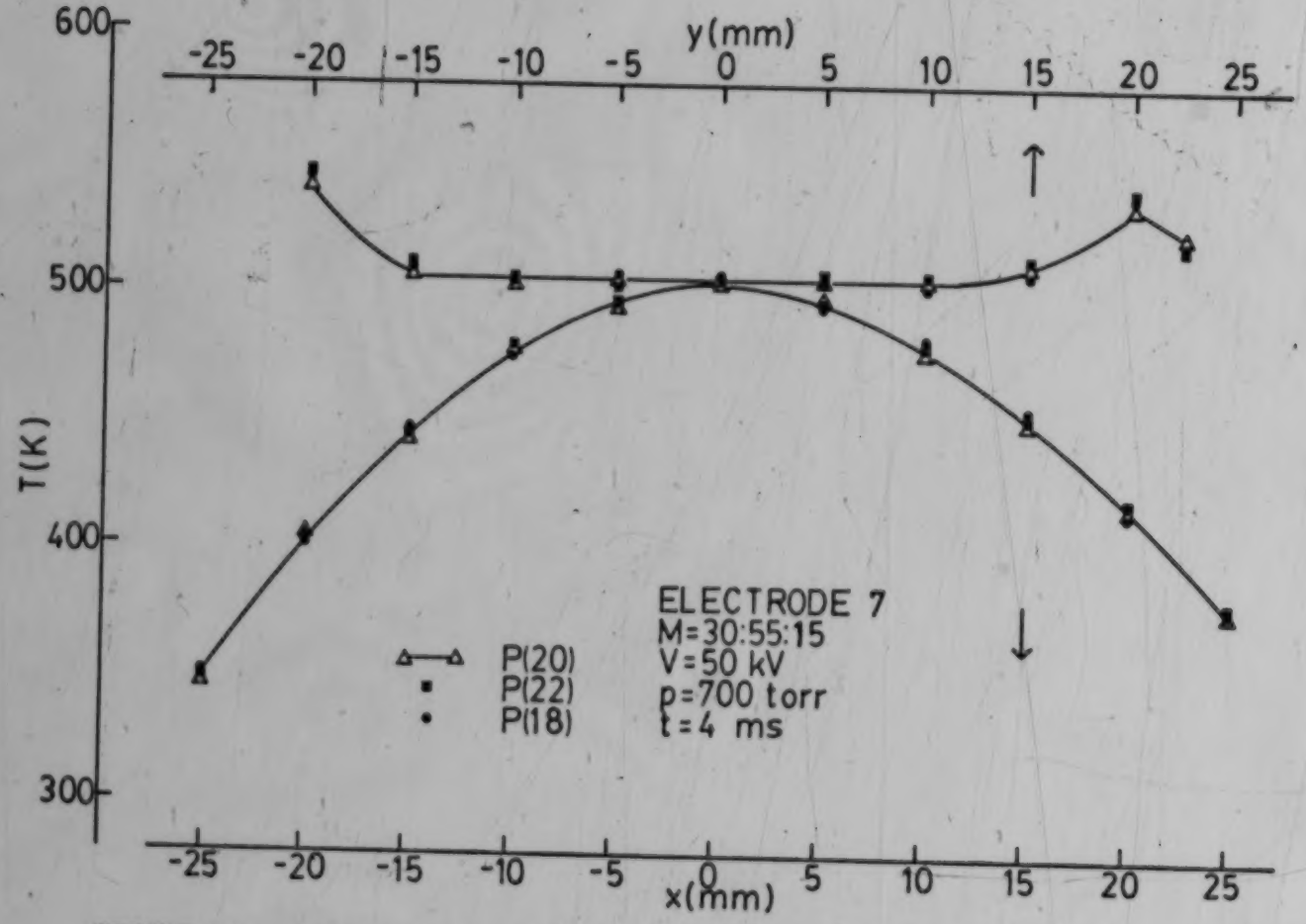

FIGURE 19. Temperature profile with x and y position.

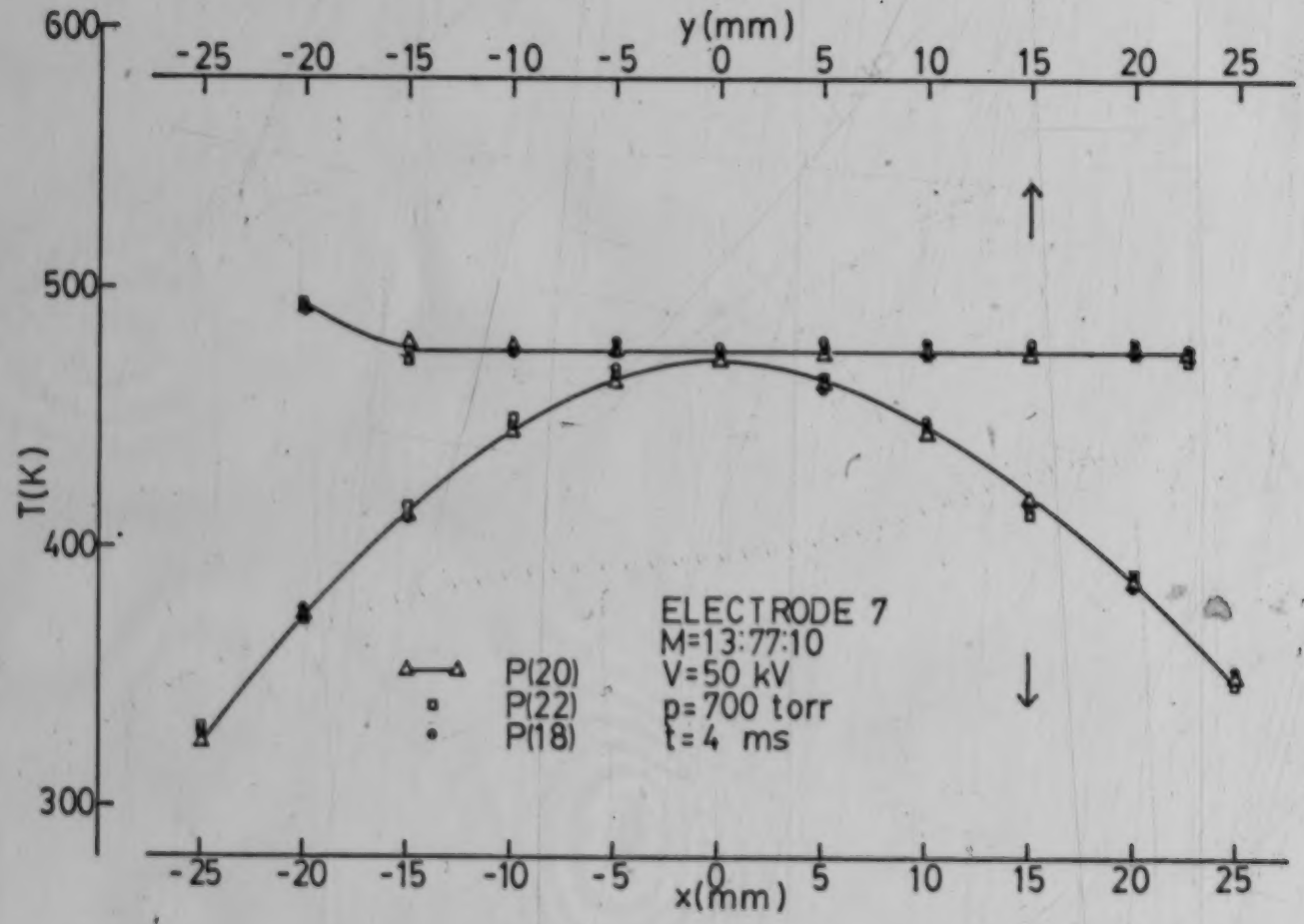

FIGURE 20. Temperature profile with x and y position.

REFERENCE

1. B.F. Gordietz, N.N. Sobolev, V.V. Sokovikov, and L.A. Shelepin, "Population Inversion of The Vibrational Levels in CO_2 Lasers", IEEE, J. Quantum Electronics, Vol. QE-4, No. 11, pp. 796-802, November 1968.
2. A.J. Beaulieu, "Transversely Excited Atmospheric Pressure CO_2 Laser", Appl. Phys. Lett., Vol. 16, pp. 504-505, June 1970.
3. M.C. Fowler, "Influence of Plasma Kinetic Processes on Electrically Excited CO_2 Laser Performance", J. Appl. Phys., Vol. 43, No. 8, pp. 3480-3487, August 1972.
4. M.C. Fowler, "Quantitative Analysis of The Dependence of CO_2 Laser Performance on Electric Discharge Properties", Appl. Phys. Lett., Vol. 18, No. 5, pp. 175-178, March 1970.
5. C.B. Moore, R.E. Wood, B.L. Hu, and J.T. Yardley, "Vibrational Energy Transfer in CO_2 Lasers", J. Chem. Phys., Vol. 46, pp. 4222-4231, June 1967.
6. A.M. Robinson, "Laser Gain Profiling with Uniform Field Electrodes", J. Appl. Phys., Vol. 47, pp. 608-615, February 1976.
7. A.M. Robinson, "Effect of Capacitance on Gain In a Transversely Pulsed CO_2 Discharge", Canadian J. Phys., Vol. 50, No. 18, pp. 2138-2148, September 1972.
8. J. Reid, E.A. Ballik and B.K. Garside, "Saturation of The Net Electron Excitation of the CO_2 (00°1) Laser Level

As a Function of Discharge Input Energy", Opt. Commun., Vol. 12, pp. 354-359, December 1974.

9. H.H. Waszink and J.A.J.M. Van Vliet, "Measurements of The Gas Temperature in CO_2-N_2-He and CO_2-N_2-H_2O-He Discharge", J. Appl. Phys., Vol. 42, pp. 3374-3379, August 1971.

10. M.C. Gower, "Measurement of Gas Temperature in a CO_2-N_2-He TEA Amplifier Using Laser Interferometry", Opt. Commun., Vol. 12, pp. 246-247, November 1974.

11. K. Dien, T. Kan and G.T. Wolga, "Gain Distribution, Population Densities, and Rotational Temperature for The (001)-(100) Rotation-Vibration Transitions in a Flowing CO_2-N_2-He Laser", IEEE, J. Quantum Electronics, Vol. QE-4, pp. 256-260, May 1968.

12. A.M. Robinson, "Gain Distribution in a CO_2 TEA Laser", Canadian J. Phys., Vol. 50, pp. 2471-2474, October 1972.

13. L.A. Weaver, L.H. Taylor and L.J. Denes, "Rotational Temperature Determinations in Molecular Gas Lasers", J. Appl. Phys., Vol. 46, No. 9, pp. 3951-3958, September 1975.

14. E.A. Ballik, B.K. Garside, J. Reid and T. Tricher, " Reduction of The Pumping Efficiency in CO_2 Lasers at High Discharge Energy", J. Appl. Phys., Vol. 46, pp. 1322-1332, March 1975.

15. J.L. Lachambre, J. Gilbert, F. Rheault, R. Fortin and M. Blanchard, "Performance Characteristic of a TEA Double-Discharge Grid Amplifier", IEEE, J. Quantum

Electronics, Vol. QE-9, pp. 459-468, April 1973.

16. G. Girard, M. Hughuet and M. Michon, "High Power Double-Discharge TEA Laser Medium Diagnostic", IEEE, J. Quantum Electronics, Vol. QE-9, pp. 426-434, March 1973.

17. L.J. Denes and L.A. Weaver, "Laser Gain Characterization of Near-Atmospheric CO_2:N_2:He Glows in a Planar Electrode Geometry", J. Appl. Phys., Vol. 44, pp. 4125-4136, September 1973.

18. R.L. Leonard, "Measurements of Small Signal Absorption at High Temperature for the 001-100 Band of CO_2", Appl. Opt., Vol. 13, No. 8, pp. 1920-1922, August 1974.

19. A. Yariv, "Introduction to Optical Electronics", New York: Holt, Rinehart and Winston, InC., 1971, p. 83.

20. A.C.G. Mitchell and M.W. Zemansky, "Resonant Radiation and Excited Atoms", London: Cambridge University Press, 1961, p. 95.

21. F.R. Petersen, D.G. McDonald, J.D. Cupp and B.L. Danielson, "Accurate Rotational Constants, Frequencies, and Wavelengths from $^{12}C^{16}O_2$ Laser Stabilized by Saturated Absorption", Proceedings of an International Conference on Laser Spectroscopy, London: Plenum Press, 1974, pp. 555-569.

22. T.Y. Chang, "Accurate Frequencies and Wavelengths of CO_2 Laser Lines", Opt. Commun., Vol. 2, pp. 77-80, July 1970.

23. J.C. Polanyi, "Vibrational-Rotational Population Inversion", Appl. Opt., Suppl. 2, Chemical Lasers, pp. 109-127,

May 1965.

24. E. Arié, N. Lacome et C. Rossetti, "Spectroscopie Par Source Laser I. Etude Experimentale des Intensités et Largeurs des Raies de la Transition 00°1-(10°0, 02°0) de CO_2", Canadian J. Phys., Vol. 50, pp. 1800-1804, August 1972.

25. L.D. Gray and J.E. Selvidge, "Relative Intensity Calculations for Carbon Dioxide I. Internal Partition Function", J. Quant. Spectroscopic Radiation Transfer, Vol. 5, pp. 291-301, February 1965.

26. G. Herzberg, "Molecular Spectra and Molecular Structure. I. Spectra of Diatomic Molecules", Princeton: Van Nostrand, 1961, p. 123.

27. G. Herzberg, "Molecular Spectra and Molecular Structure. II. Infrared and Raman Spectra of Polyatomic Molecules", Princeton: Van Nostrand, 1960, p. 503.

28. Ibid., p. 505.

29. A.C.G. Mitchell and M.W. Zemansky, "Resonant Radiation and Excited Atoms", London: Cambridge University Press, 1961, p. 161.

30. R.L. Abrams, "Broadening Coefficients for the P(20) CO_2 Laser Transition", J. Appl. Phys. Lett., Vol. 25, pp. 609-611, November 1974.

31. M. Abramowitz and I.A. Stegun, "Handbook of Mathematical Functions", New York: Dover Publication, 1965, p. 302, Formula 7.4.11.

32. C.H. Townes and A.L. Schawlow, "Microwave Spectroscopy", New York: Dover Publications, 1975, p. 368.

33. R. Ely and T.K. McCubbin Jr., "The Temperature Dependence of the Self-Broadened Half-Width of The P-20 Line in The 001-100 Band of CO_2", Appl. Opt., Vol. 9, pp. 1230-1231, May 1970.

34. A.J. Demaria, "Review of CW High-Power CO_2 Lasers", Proc. IEEE, Vol. 61, pp. 731-748, June 1973.

35. A.R. Strilchuk and A.A. Offenberger, "High Temperature Absorption in CO_2 at 10.6 μm", Appl. Opt., Vol. 13, pp. 2643-2646, November 1974.

36. S.A. Munjee and W.H. Christiansen, "Mixed Mode Contributions to Absorption in CO_2 at 10.6 μm", Appl. Opt., Vol. 12, pp. 993-996, May 1973.

37. A.M. Robinson and N. Sutton, "IR Absorption at 10.6 μm in CO_2 at Elevated Temperatures", Accepted for Publication, Appl. Opt.

38. T.Y. Chang, "Improved Uniform-Field Electrode Profiles for TEA Laser and High-Voltage Applications", Rev. Sci. Instrum, Vol. 44, No. 4, pp. 405-407, April 1973.

39. N.H. Burnett and A.A. Offenberger, "Simple Electrode Configuration for UV Initiated High-Power TEA Laser Discharges", J. Appl. Phys., Vol. 44, No. 8, pp. 3617-3618, August 1973.

40. H.J. Seguin, K. Manes and J. Tulip, "Simple Inexpensive Laboratory-Quality Rogowski TEA Laser", Rev. Sci. Instrum, Vol. 43, No. 9, pp. 1134-1139, August 1972.

41. M. Cloutier, "Computed Physical and Thermodynamic Properties of Various He-CO_2-N_2 Mixtures", Defence Research Establishment Valcartier, Courcelette, Quebec, Report DREV TN-1869/70 (unpublished).

42. F.D. Hamblin, "Abridged Thermodynamic and Thermochemical Tables", Oxford: Pergamon, 1971, p. 42.